© 2016. Published by The Company of Biologists Ltd | Journal of Cell Science (2016) 129, 2354-2367 doi:10.1242/jcs.182857

RESEARCH ARTICLE

Dictyostelium EHD associates with Dynamin and participates in phagosome maturation

Aurélie Gueho[1], Cristina Bosmani[1], Navin Gopaldass[2], Virginie Molle[3], Thierry Soldati[1] and François Letourneur[3,*]

ABSTRACT

Proteins that contain Eps15 homology domains (EHDs) in their C-terminus are newly identified key regulators of endosomal membrane trafficking. Here, we show that *D. discoideum* contains a single EHD protein (referred to as EHD) that localizes to endosomal compartments and newly formed phagosomes. We provide the first evidence that EHD regulates phagosome maturation. Deletion of EHD results in defects in intraphagosomal proteolysis and acidification. These defects are linked to early delivery of lysosomal enzymes and fast retrieval of the vacuolar H^+-ATPase in maturing phagosomes. We also demonstrate that EHD physically interacts with DymA. Our results indicate that EHD and DymA can associate independently with endomembranes, and yet they share identical kinetics in recruitment to phagosomes and release during phagosome maturation. Functional analysis of *ehd*$^-$, *dymA*$^-$ and double *dymA*$^-$*ehd*$^-$ knockout strains indicate that DymA and EHD play non-redundant and independent functions in phagosome maturation. Finally, we show that the absence of EHD leads to increased tubulation of endosomes, indicating that EHD participates in the scission of endosomal tubules, as reported for DymA.

KEY WORDS: EHD, Dynamin, *D. discoideum*, Membrane trafficking, Endosome, Phagocytosis

INTRODUCTION

C-terminal Eps15-homology-domain (EHD) proteins have recently emerged as a new family of proteins with major regulatory functions in the endocytic pathway (Naslavsky and Caplan, 2011). These proteins are characterized by the presence of an ATPase G domain followed by a coiled-coil region, and a single C-terminal Eps15-homology (EH) domain (Daumke et al., 2007; Mintz et al., 1999). The EH domain recognizes proteins with Asn-Pro-Phe (NPF) sequences (de Beer et al., 1998). Structural and functional features have revealed that EHDs are related to the Dynamin superfamily, although EHDs bind to and hydrolyze ATP rather than GTP (Daumke et al., 2007). Hence, as reported for dynamin (Takei et al., 1998), mouse EHD2 has been shown to tubulate liposomes and oligomerize in ring-like structures around these tubules (Daumke et al., 2007). In mammalian cells, there are four homologous (>70% identity) EHD proteins (EHD1–EHD4). Other organisms such as *Caenorhabditis elegans* and *Drosophila* have only a single EHD protein. No apparent homolog has been found in *Saccharomyces cerevisiae*. Several functions have been assigned to EHD proteins, with particular emphasis on protein sorting and membrane trafficking functions along the endocytic pathway (Naslavsky and Caplan, 2011). For instance, one of the most documented roles for EHD1 is in controlling cargo exit from the endocytic recycling compartment back to the plasma membrane (Caplan et al., 2002; Jovic et al., 2007; Lin et al., 2001). This is also observed for RME-1, the *C. elegans* ortholog of human EHD1, which is required for yolk receptor recycling (Grant et al., 2001). Moreover, EHD3 has been shown to contribute to cargo transport from early endosomes to the Golgi (Naslavsky et al., 2009). Surprisingly, despite EHDs being clearly implicated in cargo recycling from endosomes to several other compartments, to our knowledge, EHDs have never been shown to participate in protein retrieval from phagosomes.

The interaction of EHDs with protein partners mainly provides the molecular basis for the distinct functions of EHD-family members (Grant and Caplan, 2008; Naslavsky and Caplan, 2011; Zhang et al., 2012a). For instance, MICAL-L1, an EHD1 binding partner, has been shown to recruit collapsin response mediator protein-2 (CRMP2), which binds to dynein (Rahajeng et al., 2010). This tripartite interaction (EHD1–MICAL-L1–CRMP2) is proposed to connect EHD1 to dynein motors. Interestingly, EHD partners also include known effectors of Rab GTPases, suggesting that EHDs and Rabs might cooperate to regulate endocytic trafficking (Zhang et al., 2012b). In addition, some EHD partners facilitate EHD-dependent membrane bending, as reported for the BAR-domain-containing protein AMPH1 (also known as amphiphysin and Bin1), which interacts with EHD1 and contributes to tubule formation (Pant et al., 2009). Finally, besides their role in membrane remodeling, EHDs might serve to regulate the proper function of their binding partners. Hence, the single EHD protein in Lampreys has been reported to directly interact with dynamin, and this interaction has been shown to inhibit dynamin polymerization during synaptic vesicle formation (Jakobsson et al., 2011). The existence of dynamin–EHD complexes with similar functions in other organisms is unknown.

The amoeba *Dictyostelium discoideum* is a professional phagocyte. Genetic, microscopy and biochemical analyses have allowed the fine characterization of the endocytic and phagocytic pathways in these cells (Neuhaus et al., 2002). Similar to those in animal phagocytes, *D. discoideum* nascent phagosomes containing internalized material undergo a series of maturation events that mainly comprise extensive retrieval of non-phagosomal components (e.g. plasma membrane receptors) and fusion with endosomes and/or lysosomes to gain digestive properties (Gotthardt et al., 2002). A key step in phagosome maturation comprises the delivery of the vacuolar proton ATPase (H^+-ATPase) and hydrolytic enzymes to phagosomes. Sixty minutes after uptake, retrieval of the

[1]Department of Biochemistry, University of Geneva, Geneva CH-1211, Switzerland. [2]Department of Biochemistry, University of Lausanne, Epalinges CH-1066, Switzerland. [3]Laboratoire de Dynamique des Interactions Membranaires Normales et Pathologiques, Université de Montpellier, CNRS, UMR 5235, Place Eugène Bataillon, Montpellier Cedex 05 34095, France.

*Author for correspondence (francois.letourneur@univ-montp2.fr)

F.L., 0000-0003-2232-6127

Received 1 November 2015; Accepted 4 May 2016

Journal of Cell Science (2016) 129, 2354-2367 doi:10.1242/jcs.182857

H^+-ATPase from phagosomes results in the formation of neutral post-phagolysosomes, which eventually fuse with the plasma membrane to release undigested material. Several key players have been shown to participate in membrane fusion and fission events that are essential for H^+-ATPase cycling to phagosomes. Among those, Wiskott-Aldrich syndrome protein and SCAR Homolog (WASH), which drives actin polymerization, has been shown to be essential for H^+-ATPase recycling (Carnell et al., 2011; Park et al., 2013). In addition, Dynamin A (DymA), a *D. discoideum* homolog of dynamin notably observed on post-lysosomes (Wienke et al., 1999), is also reported to participate in early steps of the phagosome maturation process (Gopaldass et al., 2012). Indeed, deletion of *dymA* impairs phagosome acidification and F-actin binding to early phagosomes. Although DymA-driven vesicle scission could account for its role in membrane recycling during phagosome maturation, DymA might also regulate the actin cytoskeleton, as suggested by the reported interaction between dynamin and WASH in mammalian cells (Derivery et al., 2009). Consistent with this hypothesis, in *D. discoideum*, DymA is reported to interact with the actin-binding protein Abp1, and the recruitment of Abp1 to early phagosomes requires the presence of DymA (Dieckmann et al., 2010; Gopaldass et al., 2012). Interestingly, previous studies in *C. elegans* have suggested that dynamin might contribute to Rab5 recruitment to phagosomes during phagocytosis of apoptotic cells (Kinchen et al., 2008). More recently, in *C. elegans*, dynamin has been shown to form a complex with clathrin, clathrin adaptor protein complex 2 (AP2), and LST-4 (the *C. elegans* homolog of mammalian proteins Snx9, Snx18 and Snx33) to promote phagosome maturation during apoptotic cell corpse clearance (Chen et al., 2013). Therefore, dynamin might have more than one function in phagocytosis. Whether other members of the dynamin superfamily are additionally involved in phagosome maturation is unknown. Because *D. discoideum* contains a single EHD protein (referred to as EHD), this phagocytic cell is an attractive model to study the possible relationship between dynamin and EHD proteins.

In this study, we explored the localization and function of the single *D. discoideum* EHD protein in the endocytic pathway. For the first time, we report that EHD participates in phagosome maturation. Moreover, we provide evidence that EHD and DymA play non-redundant functions in this cellular process. We also reveal that EHD contributes to the scission of endosomal tubules.

RESULTS

D. discoideum contains a single EHD protein with endosomal localization

One EHD protein has been previously identified in *D. discoideum* (Daumke et al., 2007). To identify additional EHD proteins in *D. discoideum*, we searched the *D. discoideum* genome sequence database for genes that contain an EH domain (http://dictybase.org/tools/blast). Only three genes were identified, in contrast to the human genome that encodes eleven proteins with EH domains (Confalonieri and Di Fiore, 2002). The first gene, DDB_GO287325, encodes a protein (UniProtKB, Q54KI4) homologous to mammalian epidermal growth factor receptor substrate 15 (EPS15) with three copies of the EH domain in the N-terminal region, and has been previously described (Blanc et al., 2009). Next, the DDB_G0269636 (UniProtKB, Q55DJ6) gene product contains one EH domain in a central position, and was not identified in other species. The third gene, DDB_G0282233 (UniProtKB, Q54ST5), encodes a protein of 568 amino acids with a domain organization similar to that of mammalian EHD-family members and shares over 47% amino acid similarity with all human EHD proteins (EHD1–EHD4). Similar to EHD proteins in other species (Daumke et al., 2007), this *D. discoideum* protein comprises four domains: two helical domains, a G-domain that shares similarity with the dynamin G-domain and a C-terminal EH domain (Fig. 1A). Therefore, as described in *C. elegans* (Grant et al., 2001) and *D. melanogaster* (Olswang-Kutz et al., 2009), *D. discoideum* contains a single EHD protein, here referred to as EHD.

The crystal structure of mouse EHD2 has been solved and reveals that EHD proteins display a dynamin-like structural fold (Daumke et al., 2007). Based on its homology with mouse EHD2, the secondary structure assignment for *D. discoideum* EHD has been previously reported (Daumke et al., 2007). The G domain of mouse EHD2 comprises an unstructured loop that contains a KPFxxxNPF motif involved in EHD2 oligomerization (Daumke et al., 2007). *D. discoideum* EHD contains only the PF motif in this loop (Fig. 1A), like human EHD1 in which this motif is sufficient for oligomerization (Bahl et al., 2015). In mouse EHD2, an additional GPF motif has been identified in the linker region between the G domain and the EH domain and is predicted to bind to the EH domain of the opposing dimeric EHD2 molecule (Daumke et al., 2007). This motif is conserved in all mammalian EHD proteins but is replaced by an NPF motif in *D. discoideum*. Because NPF motifs are well described to have a high affinity for EH domains, this NPF motif in *D. discoideum* EHD might support EHD homodimerization.

EHD proteins in other species are known to interact with phosphoinositides (Naslavsky et al., 2007). As a first step towards the characterization of *D. discoideum* EHD, we thus assayed binding of EHD to lipids. Purified recombinant GST–EHD was incubated with a commercial nitrocellulose membrane that had been spotted with various phosphoinositides. EHD mainly interacted with phosphatidylinositol-3-phosphate [PI(3)*P*] and associated with other lipids to a lesser degree, including phosphatidylinositol-4-phosphate [PI(4)*P*], phosphatidylinositol-5-phosphate [PI(5)*P*], di- and tri-phosphorylated phosphatidylinositides (Fig. 1B). To confirm that EHD selectively binds to PI(3)*P*, we next performed liposome sedimentation assays with GST–EHD (Fig. 1C,D). In the conditions tested, about 42.5% of total GST–-EHD was observed in liposome pellets containing PI(3)*P*, whereas 20–25% of GST–EHD sedimented with liposomes containing PI(5)*P* and phosphatidylinositol-3,5-bisphosphate [PI(3,5)P_2], respectively. Binding to other phosphoinositides or liposomes composed of 30% phosphatidylserine (PS) was weaker. Increasing the concentration of PS to 100% pelleted about 70% of the total GST–EHD, whereas it did not bind to PS that had been immobilized onto nitrocellulose membranes (Fig. 1B). PS that has been incorporated into liposomes might thus better mimic PS topology in cellular membranes. No binding of GST alone to any phospholipid-containing liposomes was observed (Fig. 1C). Because PI(3)*P* is enriched on *D. discoideum* early endosomes (Clarke et al., 2010), the interaction with this phospholipid might ensure specific recruitment of EHD to these endomembranes, although other factors might also contribute to this localization. Interestingly, human EHD1 is reported to bind to PS *in vitro*, and this interaction is essential for human EHD1 recruitment to recycling endosomes (Lee et al., 2015); hence, PS might contribute in a similar way to EHD localization in *D. discoideum*.

Membrane recruitment of EHD *in vivo* was next confirmed by subcellular localization analysis. RFP-tagged EHD (RFP–EHD) was conditionally expressed in cells 24 h before confocal microscopy analysis of fixed cells (Fig. 1E,F). RFP–EHD was

Journal of Cell Science (2016) 129, 2354-2367 doi:10.1242/jcs.182857

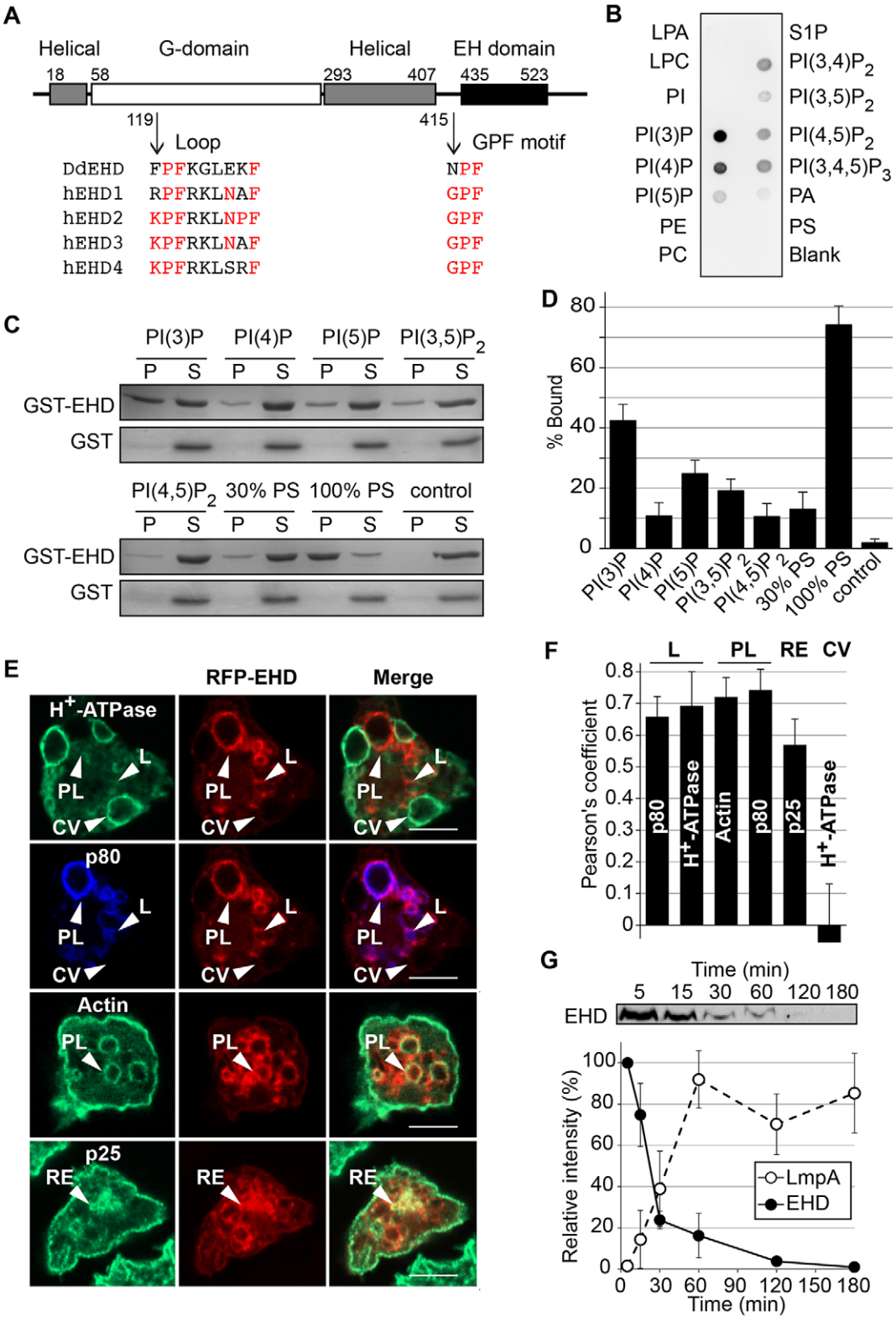

Fig. 1. See next page for legend.

excluded from the plasma membrane and the contractile vacuole, as shown by the absence of colocalization with cortical actin and the bulk of the H^+-ATPase, respectively. Conversely, RFP–EHD colocalized with recycling endosomes (p25 positive) (Charette and Cosson, 2006), lysosomes (H^+-ATPase positive, p80 positive) and post-lysosomes (H^+-ATPase negative, p80 positive, actin positive). Identical results were obtained with Myc-tagged EHD (Fig. S1A). The detection of EHD at these multiple locations suggests that EHD might participate in several steps along the endocytic pathway in *D. discoideum*. To determine the temporal localization of EHD on endosomes and evaluate its possible implication in phagocytosis, phagosomes at different stages of

Journal of Cell Science (2016) 129, 2354-2367 doi:10.1242/jcs.182857

Fig. 1. Characterization of *D. discoideum* EHD. (A) Schematic representation of EHD with known functional domains and motifs. (B) Protein-lipid overlay. GST–EHD was used to probe a commercial nitrocellulose membrane that had been spotted with various immobilized phosphoinositides. Lysophosphatidic acid (LPA), lysophosphocholine (LPC), phosphatidylinositol (PI), sphingosine 1-phosphate (S1P), phosphatidylethanolamine (PE), phosphatidylcholine (PC), phosphatidylserine (PS), phosphatidic acid (PA), phosphatidylinositol-3-phosphate [PI(3)*P*], phosphatidylinositol-4-phosphate [PI(4)*P*], phosphatidylinositol-5-phosphate [PI(5)*P*] and di- and tri-phosphorylated phosphatidylinositides are indicated. (C) Co-sedimentation of GST–EDH with liposomes composed of either 80% PC, 10% PS and 10% of the indicated phosphoinositides, or 30% PS and 70% PC (30% PS), or 100% PS. Control, no liposomes. Liposomes were incubated with GST–EHD for 1 h. After centrifugation, pellets (P) and supernatants (S) were analyzed by SDS-PAGE and Coomassie Blue staining. (D) Percentages of GST–EHD binding to liposomes were calculated after quantification of three independent experiments. Error bars represent s.d. (E) Subcellular localization of RFP–EHD. WT cells expressing RFP–EHD were processed for immunofluorescence and analyzed by confocal microscopy. Lysosomes (L; H^+-ATPase-positive, p80-positive), post-lysosomes (PL; H^+-ATPase-negative, p80-positive, actin-positive), recycling endosomes (RE; p25-positive) and contractile vacuoles (CV; H^+-ATPase-positive, p80-negative) are indicated. Scale bars: 5 µm. (F) Pearson's coefficients depicting the overlap of RFP–EHD between the indicated markers in the specified compartments (L, PL, RE and CV) were calculated with ImageJ Coloc 2. Values plotted are the mean and SD of two independent experiments (20 cells). (G) Western blot profile of EHD and LimpA (LmpA) on phagosomes containing latex beads isolated from WT cells at different times of maturation. The graph represents the quantification of three independent experiments (mean±s.d.).

maturation were purified from wild-type (WT) cells, and the presence of endogenous EHD was assessed by western blotting with an antibody against EHD (Fig. 1G). EHD was detected in early phagosomes and rapidly dissociated from maturing phagolysosomes, which were characterized by the accumulation of the endosomal protein LmpA. Previous studies have revealed the transient localization of PI(3)*P* on early phagosomes, which was detected with the PI(3)*P* biosensor GFP–2FYVE (Clarke et al., 2010; Guetta et al., 2010) and the arrestin-related protein AdcA (Guetta et al., 2010). Although binding to PI(3)*P* might explain the temporal profile of EHD phagosomal recruitment, additional interactions with other proteins and/or lipids might also control EHD dynamics. In macrophages, PS is continuously maintained at a high level in phagosomes during the whole maturation process through fusion with PS-enriched endocytic compartments (Yeung et al., 2009). Whether such a constant PS level is observed in *D. discoideum* phagosomes is unknown and, if verified, it would not match EHD dynamics in phagosomes.

EHD interacts with DymA

As a first step towards deciphering the role of EHD in the endocytic pathway of *D. discoideum*, a yeast two-hybrid screen was performed using the EH domain as a bait. Among identified preys (Table S1), DymA was isolated 43 times with a very high confidence score for the interaction. The domain of interaction between EHD and DymA was deduced from sequences of overlapping DymA preys and resided in a peptide of 33 residues (D548 to Q580) that contains an NPF motif recognized by EH domains. This short peptide is included in the Glu-Asp-Ser-rich region of DymA (QNS region), which showed no amino-acid sequence similarity with members of the dynamin family in any other species (Wienke et al., 1999). Thus, *D. discoideum* DymA appears to be the only dynamin homolog across species with an NPF motif. Although our yeast two-hybrid screen revealed other interesting candidates, we chose to focus on DymA mainly owing to its role in membrane trafficking and the reported interaction between EHD and dynamin in Lamprey (Jakobsson et al., 2011).

To verify the interaction between EHD and DymA, we first performed GST pulldown assays (Fig. 2A). Fusion proteins made between GST and EHD were immobilized onto glutathione agarose beads and incubated with *D. discoideum* cell lysates. Bound proteins were revealed by western blot with an anti-DymA antibody. Full-length EHD (GST–EHD) and the EH domain alone (GST–EH) interacted with DymA. In contrast, DymA was not detected using GST alone or EHD in which the EH domain had been deleted (GST–EHD-ΔEH), confirming that the EH domain of EHD is responsible for the interaction with DymA. This was further demonstrated by mutation of the NPF motif in GFP-tagged DymA (P573G,F574S double mutation, GFP–DymA-NGS mutant), which fully abolished DymA binding to GST–EHD (Fig. 2B). Next, the interaction between EHD and DymA was assessed by performing immunoprecipitation experiments. Lysates from cells overexpressing GFP–DymA were immunoprecipitated with beads coupled to an antibody against GFP. Immunoblotting of eluted beads with an antibody against EHD revealed the presence of EHD, consistent with an *in vivo* interaction between EHD and DymA (Fig. 2C). Co-precipitation between endogenous DymA and GFP-tagged EHD was also observed (Fig. S1B).

Taken together, these data suggest that EHD and DymA colocalize in endosomal compartments. To test this hypothesis, RFP–EHD and GFP–DymA were coexpressed in WT cells, and fixed cells were observed with confocal microscopy. As shown in Fig. 2Da, both proteins colocalized around vacuoles as well as in punctate structures in close vicinity to these endomembranes (indicated by arrowheads). Interestingly, despite the physical interaction between EHD and DymA revealed above, both proteins were also present on vacuoles independently of each other. Indeed, in the absence of DymA (*dymA*$^-$ knockout cells), RFP–EHD still localized to p80- and p25-positive vacuoles (Fig. 2Db,Dc). Reciprocally, deletion of the gene encoding EHD (*ehd*$^-$ cells were further characterized hereafter) did not modify GFP–DymA cellular distribution, although a slight diffuse cytoplasmic staining was also observed (Fig. 2Dd). Moreover, the GFP–DymA-NGS mutant, which does not interact with EHD (Fig. 2B), still correctly localized to p80-positive vacuoles when expressed in *dymA*$^-$ cells (Fig. 2De).

To test for a possible co-recruitment of EHD and DymA to phagosomes, we next analyzed the dynamics of these proteins during phagosome maturation. Cells coexpressing RFP–EHD and GFP–DymA were incubated with latex beads and imaged by using time-lapse video microscopy (Fig. 3). As observed in Fig. 3 (see Movie 1) (Fig. 3B), RFP–EHD and GFP–DymA proteins appeared simultaneously and were recruited extremely rapidly to phagosomes, reaching a peak at about 5 min, and then concomitantly released during phagosome maturation. These similar dynamics of both proteins on maturing phagosomes might thus reflect coordinated functions of these two proteins.

EHD is essential for optimal phagosome maturation

To determine the function of EHD in the endocytic pathway and to further explore the possible interplay between EHD and DymA, we decided to inactivate the gene encoding EHD both in WT and *dymA*$^-$ cells. Systematic morphological and functional analysis of the endocytic pathway did not reveal any major defect resulting from the absence of EHD in WT cells or aggravation of *dymA*$^-$ phenotypes in *dymA*$^-$*ehd*$^-$ cells (Figs S1C–G,S2 and S3).

DymA has been previously shown to play a major role in maturation of early phagosomes (Gopaldass et al., 2012). The interaction of EHD with DymA prompted us to test whether EHD might share similar functions. We first measured proteolytic activity

Journal of Cell Science (2016) 129, 2354-2367 doi:10.1242/jcs.182857

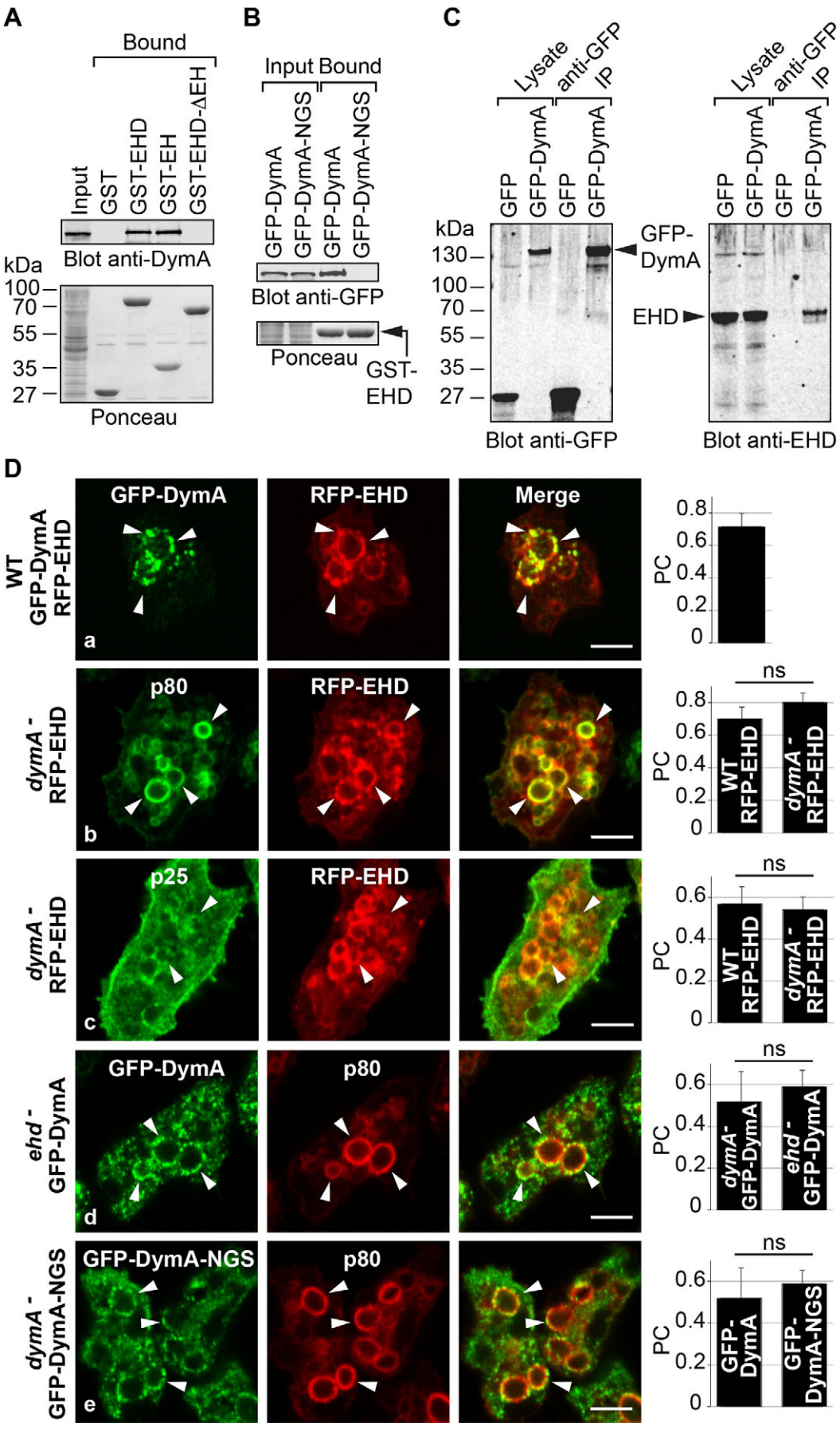

Fig. 2. See next page for legend.

Journal of Cell Science (2016) 129, 2354-2367 doi:10.1242/jcs.182857

Fig. 2. EHD interacts with DymA. (A) GST pulldown analysis. The indicated GST fusion proteins bound to glutathione beads were incubated with WT cell lysates. Bound proteins were revealed by western blot analysis with an anti-DymA antibody (upper panel). Full-length EHD (GST–EHD) and the EH domain of EHD (GST–EH) bound to DymA. Ponceau staining of the blotted membrane (lower panel) was used as a loading control. (B) GST–EHD beads were incubated with lysates of the indicated cells, and bound proteins were revealed with an anti-GFP antibody (upper panel). Lower panel shows Ponceau staining of the blotted membrane. (C) Co-immunoprecipitation between GFP–DymA and EHD. Lysates of cells expressing GFP alone or GFP–DymA where incubated with beads coupled to an anti-GFP antibody (IP). Bound proteins were revealed by immunoblotting with anti-EHD and anti-GFP antibodies as indicated. (D) Confocal fluorescence microscopy of fixed cells. (a) Colocalization between DymA and EHD in WT cells coexpressing GFP–DymA and RFP–EHD (arrowheads indicate colocalization); (b,c) RFP–EHD localization to p80- and p25-positive vacuoles in *dymA*$^{-}$ cells; (d) GFP–DymA localization to p80-positive vacuoles in *ehd*$^{-}$ cells; (e) GFP–DymA-NGS localization to p80-positive vacuoles in *dymA*$^{-}$ cells. Pearson's coefficients (PC) were calculated using ImageJ Coloc 2. Values plotted and shown next to each image are the mean±s.d. of two independent experiments (20 cells). ns, not significant. Scale bars: 5 µm.

inside phagosomes in living cells. Cells were fed with beads coupled to Alexa-Fluor-594 and to bovine serum albumin (BSA) labeled with DQ Green at a self-quenching concentration. In this assay, BSA proteolysis in phagosomes releases DQ Green and subsequent dequenched fluorescence emission is recorded (Sattler et al., 2013). We observed that protease activity was very decreased in *ehd*$^{-}$ cells compared to that in WT cells (Fig. 4A). This defect was even more marked than that in *dymA*$^{-}$ cells and was further increased in *dymA*$^{-}$*ehd*$^{-}$ double mutants. Measuring the activity of various intracellular hydrolases (Fig. S3E–H) failed to reveal any decrease between mutants and WT cells. On the contrary, in mutants lacking DymA, the overall activity was higher than that measured in WT cells. Therefore, the defect in phagosomal proteolytic activity is likely not to be the result of hydrolases being absent from the cells, but can be explained either by a suboptimal phagosomal pH or the mis-trafficking of the proteases that are normally delivered to maturing phagosomes.

An essential step in phagosome maturation is the rapid acidification of newly formed phagosomes, followed by their neutralization before exocytosis of undigested material (Maniak, 2003). Thus, the endosomal and phagosomal pH has been shown to reach values around 4 after 45–50 min, and reneutralize to about 6 after 120–180 min (Aubry et al., 1993; Maniak, 2003; Marchetti et al., 2009; Sattler et al., 2013). To determine whether this pH profile during phagosome maturation is affected in the absence of EHD, we monitored phagosomal pH as previously described (Sattler et al., 2013). Monolayers of cells in 96-well plates were fed with beads labeled with the pH-sensitive fluorochrome fluorescein isothiocyanate (FITC) and the pH-insensitive fluorochrome Alexa-Fluor-594. The fluorescent emissions of both fluorochromes were recorded with a plate reader, and relative pH kinetics were analyzed by plotting the ratios of FITC and Alexa-Fluor-594 fluorescence values as a function of time (Fig. 4B). The observed ratios in WT cells correspond to an initial acidification minimum of around pH 4 that was reached after 53 min, followed by a reneutralization over the next 3 h (Fig. 4B). In *ehd*$^{-}$ cells, this profile was substantially different, because the population of maturing phagosomes was less acidic, reaching its minimum only after 63 min, but the kinetics of reneutralization were similar to those in WT cells. Interestingly, this pH profile was less affected than that in *dymA*$^{-}$ cells (Fig. 4B) (Gopaldass et al., 2012). However, the absence of both EHD and DymA proteins resulted in a dramatic decrease in the rate and extent of acidification because a minimum similar to that measured in *ehd*$^{-}$ cells was reached after 149 min, and full neutralization did not occur even after 4 h.

The cumulative defects in phagosomal proteolysis and pH kinetics in *dymA*$^{-}$*ehd*$^{-}$ double mutants suggested that DymA and EHD play non-redundant functions in these two processes. This hypothesis was confirmed by the fact that overexpression of GFP–DymA in *ehd*$^{-}$ cells did not restore normal phagosomal proteolysis and the normal pH profile but, instead, worsened these defects to an extent even more dramatic than that observed in *dymA*$^{-}$*ehd*$^{-}$ cells (Fig. 4C,D). Synthetic aggravation of a phenotype in a mutant cell through overexpression of another wild-type gene is widely exploited in genetic screens and usually indicates that two gene products function in the same pathway or associate in a protein complex (Prelich, 2012). The enhanced inhibition observed here is thus consistent with DymA and EHD co-functioning during phagosome maturation. Next, to determine the role of the interaction between DymA and EHD, we assessed whether a DymA mutant that was unable to bind to EHD (GFP–DymA-NGS) could rescue defects in *dymA*$^{-}$ cells. Phagosomal proteolysis and pH profile analyses revealed that both GFP–DymA-NGS and GFP–DymA rescued the *dymA*$^{-}$ phenotype to equal extents (Fig. 4E,F). Thus, the physical interaction between DymA and EHD appears to be dispensable for DymA functions in the phagosomal maturation processes analyzed, although we cannot formally exclude that the DymA–EHD interaction, undetected under our experimental conditions, might still occur independently of the NPF motif in DymA.

Sequential delivery and recycling of the vacuolar H^+-ATPase to and from phagosomes accounts for the acidification and neutralization steps accompanying maturation (Carnell et al., 2011; Clarke et al., 2010). Thus, impaired acidification of phagosomes in *ehd*$^{-}$ cells might be due to either defective H^+-ATPase targeting to phagosomes or faster retrieval from phagosomes. To distinguish between these two possibilities, we next analyzed the dynamics of GFP-tagged M subunit of the H^+-ATPase (GFP–VatM) during maturation of phagosomes with time-lapse video microscopy (Fig. 5). We observed that GFP–VatM delivery to phagosomes in *ehd*$^{-}$ and WT cells occurred at similar rates. In contrast, GFP–VatM retrieval from phagosomes had already started, on average, 15 min after delivery in *ehd*$^{-}$ cells, instead of at 25 min in WT cells, and was considerably faster in mutant cells (Fig. 5). These results strongly suggest that premature and faster rates of H^+-ATPase retrieval from phagosomes might explain the abnormal pH profile observed during phagosome maturation in the absence of EHD.

To determine whether the defect in the dynamics of phagosomal H^+-ATPase transport reflects a more general defect in phagosome maturation in *ehd*$^{-}$ cells, we isolated phagosomes from WT and *ehd*$^{-}$ cells at different steps of the maturation process. The temporal profiles of several phagosomal proteins were then monitored by western blotting analysis (Fig. 6). As previously reported (Gopaldass et al., 2012), DymA and MyoB mainly associated with nascent and newly formed phagosomes, and were rapidly dissociated during phagosome maturation in WT cells (Fig. 6). In the absence of EHD, DymA and MyoB were still efficiently recruited onto nascent phagosomes, further confirming EHD-independent membrane recruitment of DymA, as first suggested by the results of confocal microscopy studies (Fig. 2D). In contrast, DymA and MyoB were more rapidly released from maturing phagosomes in *ehd*$^{-}$ cells than in WT cells. Because it has been suggested that MyoB and DymA control the recycling of the H^+-ATPase from phagosomes (Gopaldass et al., 2012), the early departure of MyoB and DymA from phagosomes in *ehd*$^{-}$ cells might thus explain the accelerated retrieval of the H^+-ATPase and

Journal of Cell Science (2016) 129, 2354-2367 doi:10.1242/jcs.182857

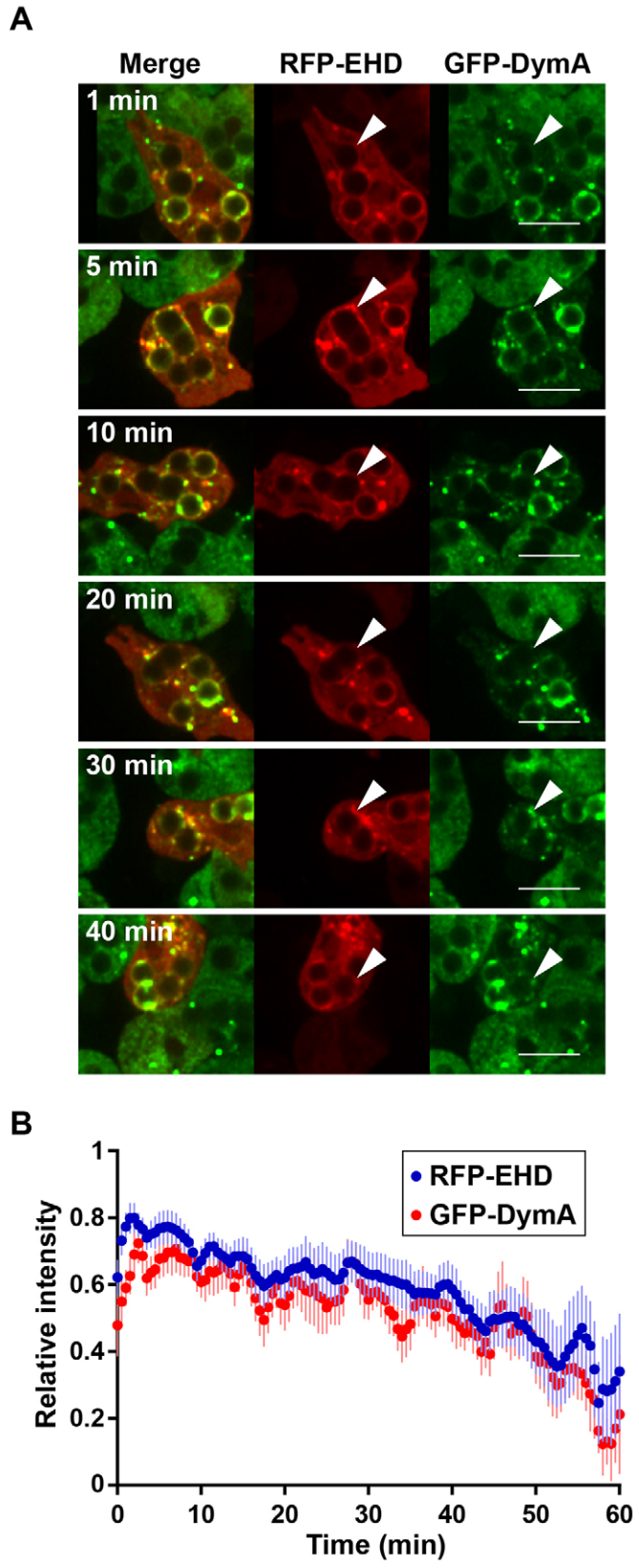

Fig. 3. Time-lapse video microscopy analysis of RFP–EHD and GFP–DymA recruitment on phagosomes. Cells co-expressing RFP–EHD and GFP–DymA were fed with latex beads and imaged every minute with a spinning disk confocal microscope. (A) Snapshots of a movie (Movie 1) showing the temporal recruitment of RFP–EHD and GFP–DymA to a phagosome. Arrowheads indicate phagosomes containing latex beads. Scale bars: 10 µm. (B) The fluorescence intensities of RFP–EHD (blue) and GFP–DymA (red) around phagosomes from movies of four independent experiments, and at least 20 phagosomes were quantified with ImageJ and normalized to the maximum fluorescence intensity of RFP–EHD and GFP–DymA, respectively, for each phagosome. RFP–EHD and GFP–DymA proteins appear to be synchronously recruited onto and released from phagosomes containing latex beads.

the aberrant acidification observed in *ehd*$^{-}$ cells (Figs 4B and 5). Surprisingly, EHD showed similar release from phagosomes in *dymA*$^{-}$ and WT cells (Fig. S3I), indicating that the transport profile of EHD is not affected by the absence of DymA. Note that deletion of *dymA* has been reported to result in massive recruitment of MyoB to maturing phagosomes (Gopaldass et al., 2012) in contrast to the MyoB early release observed here in *ehd*$^{-}$ cells.

Interestingly, analysis of proteins recruited during late stages of phagosome maturation (Fig. 6) revealed earlier phagosomal delivery of the lysosomal hydrolase Cathepsin D in *ehd*$^{-}$ cells, whereas the delivery of LmpA was very similar in *ehd*$^{-}$ and WT cells (although earlier delivery of LmpA was noticed in some experiments). Several delivery and recycling steps occur during phagosome maturation, and notably different subsets of hydrolases are delivered in this process. Accordingly, LmpA and Cathepsin D display different temporal delivery profiles, indicating that these proteins are delivered through fusion with distinct endolysosomal populations (Gotthardt et al., 2002). Hence, the heterogeneity of lysosomes might explain why Cathepsin D and LmpA delivery to phagosomes were not affected to the same extent in the absence of EHD. Taken together, these results indicate that the overall phagosome maturation process is accelerated in the absence of EHD. Thus, EHD might control the appropriate timing of sequential molecular events (e.g. vesicle scission) during phagosome maturation.

Deletion of *ehd* increases tubulation of endosomes

DymA has been previously shown to control the scission of tubules formed at the surface of endosomes (Gopaldass et al., 2012). Because Dynamin and EHD proteins share structural and functional features (Daumke et al., 2007), we next assessed the interplay between DymA and EHD in the dynamics of endosomal tubules. Cells were incubated overnight in culture medium containing tetramethylrhodamine B isothiocyanate (TRITC)–dextran to load all endo-lysosomal compartments and observed by using spinning disk video microscopy. Because endosomal tubules are highly dynamic structures, a high frame rate of one image per second, limiting the observation to a single focal plane, was used. In addition, to allow the observation of a high number of tubules in one focal plane, cells were flattened by overlaying them with a thin agar sheet. As previously described (Gopaldass et al., 2012), *dymA*$^{-}$ cells showed an increased number of tubules compared to WT cells, and these tubules were longer and persisted for extended periods of time (Fig. 7A–D; Movies 4 and 5). Remarkably, similar defects were also observed in *ehd*$^{-}$ cells (Fig. 7A–D; Movie 6). These alterations were not intensified upon deletion of both *dymA* and *ehd* genes (Fig. 7A–D; Movie 7). The absence of cumulative defects in *dymA*$^{-}$*ehd*$^{-}$ cells suggested that DymA and EHD might share similar functions in the scission of endosomal tubules. Note that tubules emanating from Lucifer-Yellow-filled pinosomes were labeled by RFP–EHD (Fig. 7E; Movie 8), in agreement with a role of EHD in endosomal tubule dynamics. Finally, transmission electron microscopy analysis of endosomal tubules did not reveal any marked ultrastructural differences in the tubular structures observed in WT and mutant cells (Fig. S4).

Journal of Cell Science (2016) 129, 2354-2367 doi:10.1242/jcs.182857

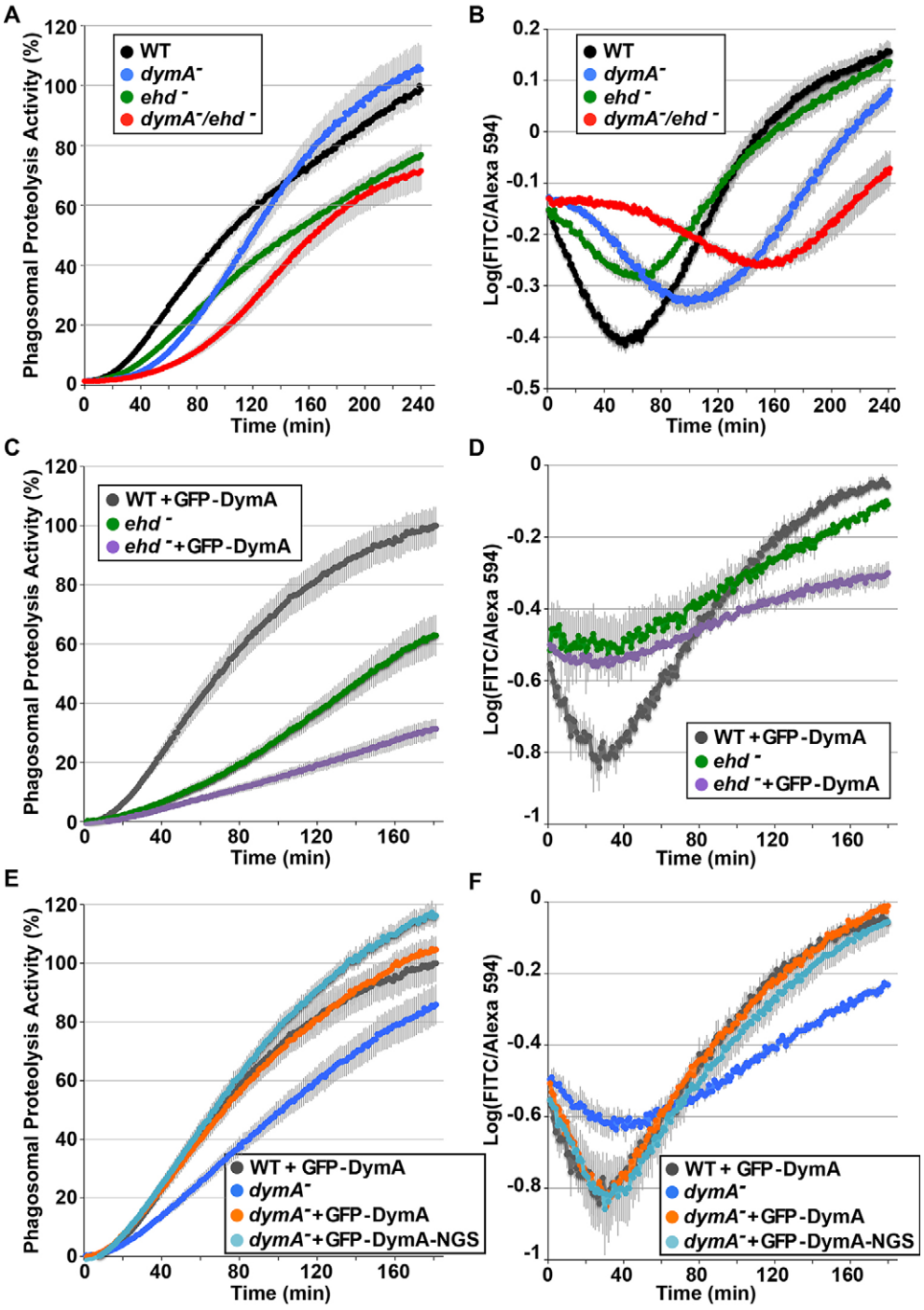

Fig. 4. Phagosomal proteolytic activities and pH profiles in mutant cells. (A) Phagosomal proteolysis activity in WT (black), *dymA*$^{-}$ (blue), *ehd*$^{-}$ (green) and *dymA*$^{-}$*ehd*$^{-}$ (red) cells. To measure phagosomal proteolysis activity, cells were fed with beads labeled with BSA–DQ-Green and Alexa-Fluor-594. Fluorescence is quenched on beads but increases upon BSA proteolysis and release of fluorophores. Phagosomal proteolysis activity is plotted as the ratio of DQ Green fluorescence to that of Alexa-Fluor-594 normalized to the ratio observed for WT cells at 240 min. (B) Phagosomal pH profile during phagosome maturation in the indicated cells. Cells were fed with beads labeled with FITC (pH sensitive) and Alexa-Fluor-594 (pH insensitive), and the ratios of the fluorescence intensity of FITC to that of Alexa-Fluor-594 were calculated. (C,D) Phagosomal proteolysis activity and pH dynamics assayed in *ehd*$^{-}$ cells (green), *ehd*$^{-}$ cells expressing GFP–DymA (*ehd*$^{-}$+GFP–DymA, purple) and WT cells expressing GFP–DymA (gray). (E,F) Phagosomal proteolysis activity and pH dynamics assayed in *dymA*$^{-}$ cells (blue) and *dymA*$^{-}$ cells expressing either GFP–DymA (orange) or GFP–DymA-NGS (light blue), and WT cells expressing GFP–DymA (gray). Curves in A–C,E and D,F represent, respectively, the mean±s.e.m. of seven and three independent experiments. Note that differences between the ranges of the ratios observed in A,B and (C–F) result from disparities in batches of custom-made reagents because ratio values depend on the coupling efficiency of BSA–DQ-Green and Alexa-Fluor-594, and FITC and Alexa-Fluor-594 to beads (Sattler et al., 2013).

DISCUSSION

In this study, we report the function of the single EHD protein expressed in the model organism *D. discoideum*. We provide the first evidence that EHD regulates phagosome maturation and endosomal tubule formation. Dynamin (DymA) has previously been shown to control these two processes (Gopaldass et al., 2012). We therefore analyzed the functional relationship between EHD and DymA. We demonstrate here that these proteins physically interact and play non-redundant independent functions in phagocytosis.

EHD controls phagosome maturation

Making use of several protein–protein interaction assays, we reveal here a physical interaction between DymA and EHD. This observation is in agreement with the initial report of a direct binding between EHD and dynamin in Lamprey axons (Jakobsson et al., 2011), and suggests that this interaction might also exist in other organisms. What are the biological consequences of the formation of DymA–EHD complexes? We first examined whether this interaction might control the membrane association of both DymA and EHD. Here, we demonstrated that DymA and EHD are recruited to endosomal membranes independently of each other. Indeed, both proteins are properly localized in the absence of the other. Membrane recruitment of both DymA and EHD might occur through direct binding to phosphoinositides. Indeed, DymA has been shown to bind to several phosphoinositides including PI(3)*P*, PI(4)*P*, PI(5)*P*, PI(3,5)P_2, phosphatidylinositol-4,5-bisphosphate

Journal of Cell Science (2016) 129, 2354-2367 doi:10.1242/jcs.182857

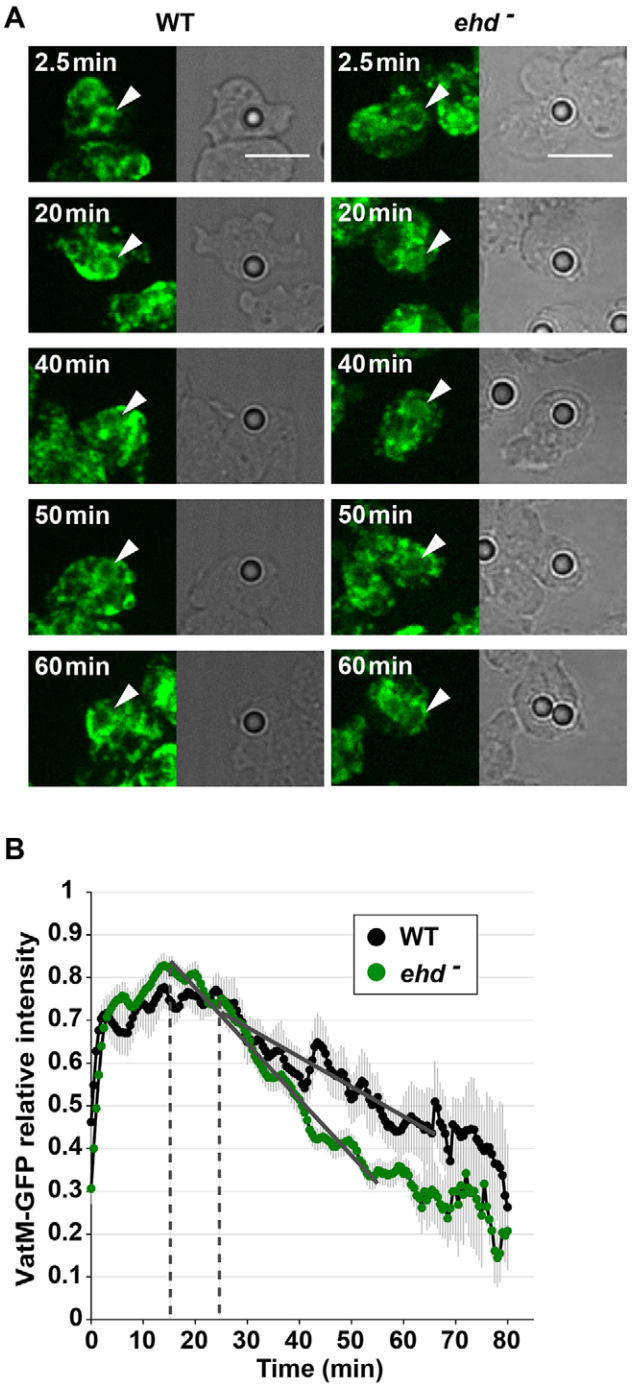

Fig. 5. VatM dynamics in mutant cells. (A) Snapshots of movies showing the temporal recruitment of the H^+-ATPase (VatM–GFP) to phagosomes in WT and *ehd*$^-$ cells (Movies 2 and 3, respectively). Cells were fed with latex beads and imaged every minute with a spinning disk confocal microscope. Scale bars: 10 µm. (B) VatM–GFP fluorescence intensity around phagosomes in WT (black) and *ehd*$^-$ cells (green) was measured with ImageJ and then normalized to the maximum fluorescence intensity for each phagosome. Curves represent the mean of normalized fluorescence intensities and s.e.m. from three movies from three independent experiments for WT cells, and eight movies from five independent experiments for *ehd*$^-$ cells. Data for the retrieval step were best fitted using linear regression. Regression lines (gray) and the retrieval starting time point (dotted lines) are indicated. Line slopes are -7.06×10^{-3} (R^2=0.89) and -1.34×10^{-2} (R^2=0.98) for WT and *ehd*$^-$ cells, respectively, and are significantly different ($P<10^{-4}$; ANCOVA test). Arrowheads indicate phagosomes containing latex beads.

[PI(4,5)P_2] and phosphatidylinositol-3,4,5-trisphosphate (Klockow et al., 2002). Although EHD bound to the same variety of phosphoinositides as DymA, EHD displayed a stronger interaction with PI(3)*P* (Fig. 1B–D), and this selective binding might thus explain its recruitment to early phagosomes. Still, the temporal profile of EHD recruitment to phagosomes only approximately matched the reported dynamics of PI(3)*P* on early phagosomes. Indeed, PI(3)*P* labeling is lost a few minutes after phagosome closure (Clarke et al., 2010), whereas it took about 20 min to observe a 50% reduction in EHD presence on phagosomes (Fig. 1G). This implies that other proteins might also control EHD membrane recruitment. Taken together, these results suggest that DymA–EHD complexes might attach to membranes through either of the proteins (or even both), or through the interaction with other proteins such as Abp1, which has been shown to bind to DymA with high affinity (Dieckmann et al., 2010). The yeast two-hybrid candidate interaction between EHD and AbpF (Table S1) might support this hypothesis. Further time-lapse video microscopy studies revealed that DymA and EHD are simultaneously recruited and retrieved during phagosome maturation. Although technical limitations (e.g. rate of acquisition) might prevent assessment of the actual sequence of events, this result strongly suggests that DymA and EHD might be recruited together to phagosomes and, afterwards, simultaneously released from membranes, thus ruling out any clear control of membrane attachment or release by either protein.

Next, we examined whether the DymA–EHD interaction ensures a possible functional interdependence between these proteins. Analysis of *ehd*$^-$ cells revealed a role of EHD in phagosome maturation. Because DymA has also been shown to control this process (Gopaldass et al., 2012), the physical interaction between DymA and EHD indicates possible interconnected functions shared between these proteins. Contrary to this hypothesis, several lines of evidence demonstrate that DymA and EHD display non-redundant and independent functions in phagosome maturation. Indeed, analysis of the intraphagosomal pH profile, the dynamics of the vacuolar H^+-ATPase and the content of key proteins in phagosomes revealed that *ehd*$^-$ cells showed faster maturation of phagosomes compared to WT cells (Figs 4–6). Accordingly, *ehd*$^-$ cells exhibited faster release of DymA and MyoB from maturing phagosomes (Fig. 6). In contrast, *dymA* deletion was reported to inhibit early stages of phagosome maturation resulting in phagosome acidification defects (Gopaldass et al., 2012). This premature and fast phagosome maturation in the absence of EHD suggests that the actual function of EHD is to regulate key steps in phagosome maturation. Finally, we showed that DymA could not substitute for EHD (Fig. 4C,D) and that EHD binding to DymA is not required for DymA functions because mutation of the NPF motif in DymA impaired EHD binding without any functional defects (Figs 2B and 4E,F). Taken together, these results indicate no apparent functional connections between these proteins in phagosome maturation despite their physical interaction.

Mechanisms of EHD function in phagosome maturation

What is the actual function of EHD in phagosome maturation? Phagosomes undergo a series of finely tuned vesicular fusion and fission events during maturation (Fairn and Grinstein, 2012; Gotthardt et al., 2002). Therefore, EHD might control the timely delivery and/or retrieval of key proteins involved in phagosome maturation. Owing to inferred membrane remodeling properties typically observed for EHDs in other organisms, *D. discoideum* EHD might be directly involved in the budding of vesicles that recycle proteins from maturing phagosomes. Alternatively, EHD

Journal of Cell Science (2016) 129, 2354-2367 doi:10.1242/jcs.182857

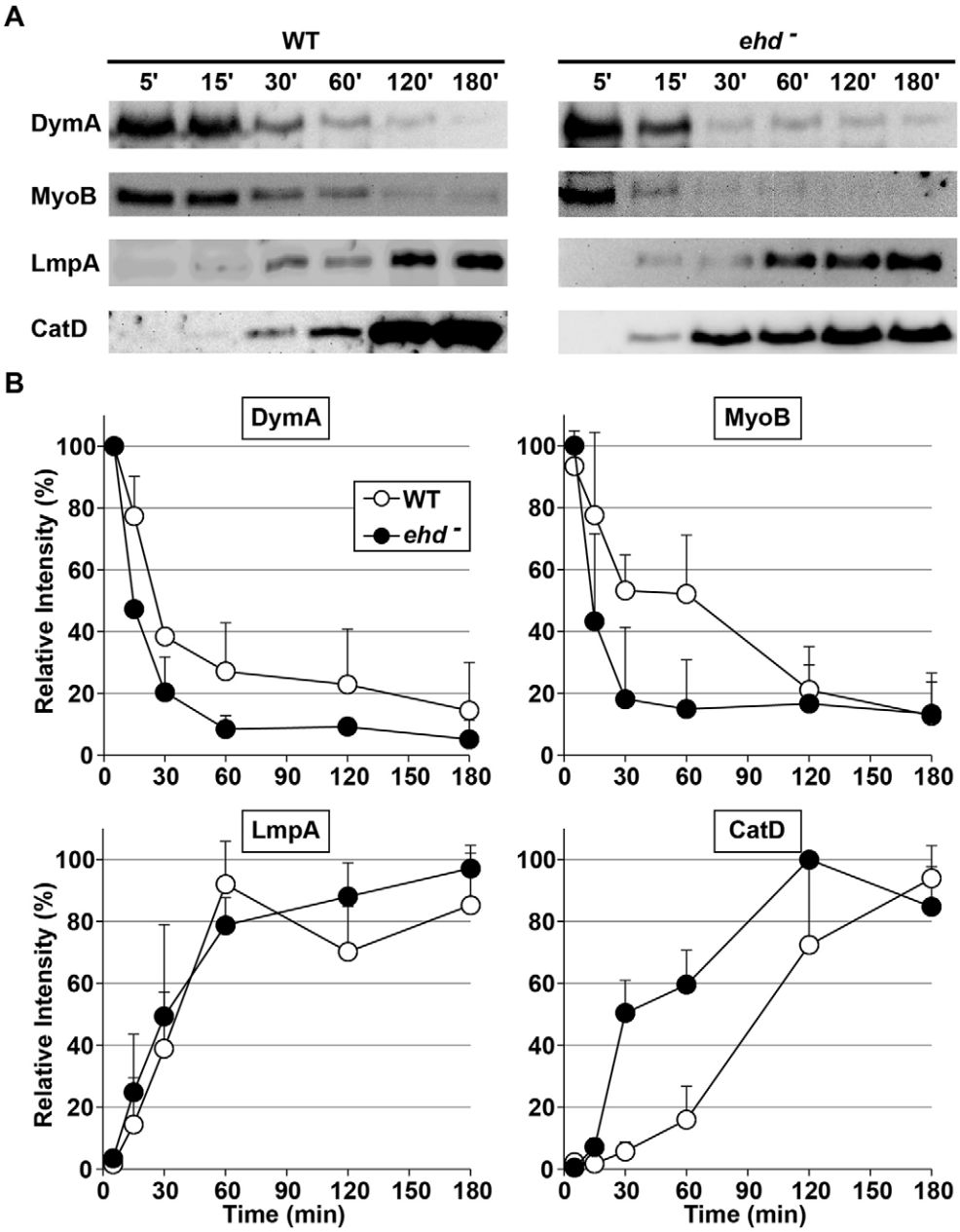

Fig. 6. Phagosome maturation in *ehd*⁻ cells. (A) Western blot profiles of DymA, MyoB, LmpA and CatD contents in phagosomes containing latex beads that were isolated at different times of maturation in WT and *ehd*⁻ cells. (B) Quantification from three independent western blot profiles (mean±s.d.) obtained as described in A. Results are expressed as the percentage of the maximal signals obtained (open circles, WT cells; closed circles, *ehd*⁻ cells).

might play an indirect role by controlling the function of EHD-binding partners that regulate the retrieval of cargo from phagosomes. Several protein complexes, including CORVET and HOPS tethering complexes and retromer, are thought to contribute to phagosomal protein recycling (Fairn and Grinstein, 2012). For instance, the retromer complex is reported to participate in phagocytosis of apoptotic cells in *C. elegans* (Chen et al., 2010). Interestingly, EHD1 has been shown to regulate endosomal retrograde transport mediated by the retromer complex through its interaction with rabankyrin-5 (Zhang et al., 2012c). Accordingly, we hypothesize that *D. discoideum* EHD controls retromer-mediated retrieval through interaction with an as-yet unidentified functional homolog of Rank-5. Furthermore, our yeast two-hybrid screen suggests that EHD might interact with a protein that is similar to human VPS33B-interacting protein (Table S1). The VPS33B-interacting protein (also known as VIPAS39, C14orf133, SPE-39, VIPAR and VPS16B) is part of the CORVET complex and regulates lysosomal delivery (Zhu et al., 2009). Interestingly, mutation in the full-of-bacteria (fob) gene, which encodes *Drosophila* VPS16B, results in defects in the fusion of phagosomes with lysosomes (Akbar et al., 2011). Thus, the hypothetical role of EHD in the regulation of the *D. discoideum* homolog of VPS16B and CORVET during phagosome maturation might be worth exploring.

Besides its hypothetical role in retromer-dependent retrieval, EHD might regulate other protein recycling mechanisms that are at play during phagosome maturation. For instance, beyond their role in clathrin-independent endocytosis, new trafficking functions have emerged for flotillins (Meister and Tikkanen, 2014). Remarkably, flotillins have been shown to regulate sorting and recycling of transferrin receptor and E-cadherin from tubulovesicular recycling compartments that are positive for Rab11a, SNX4 and EHD1 back to the plasma membrane (Solis et al., 2013). Although flotillins are recruited onto mature phagosomes both in mammals and *D. discoideum* (Gotthardt et al., 2006; Jenne et al., 1998), their

Journal of Cell Science (2016) 129, 2354-2367 doi:10.1242/jcs.182857

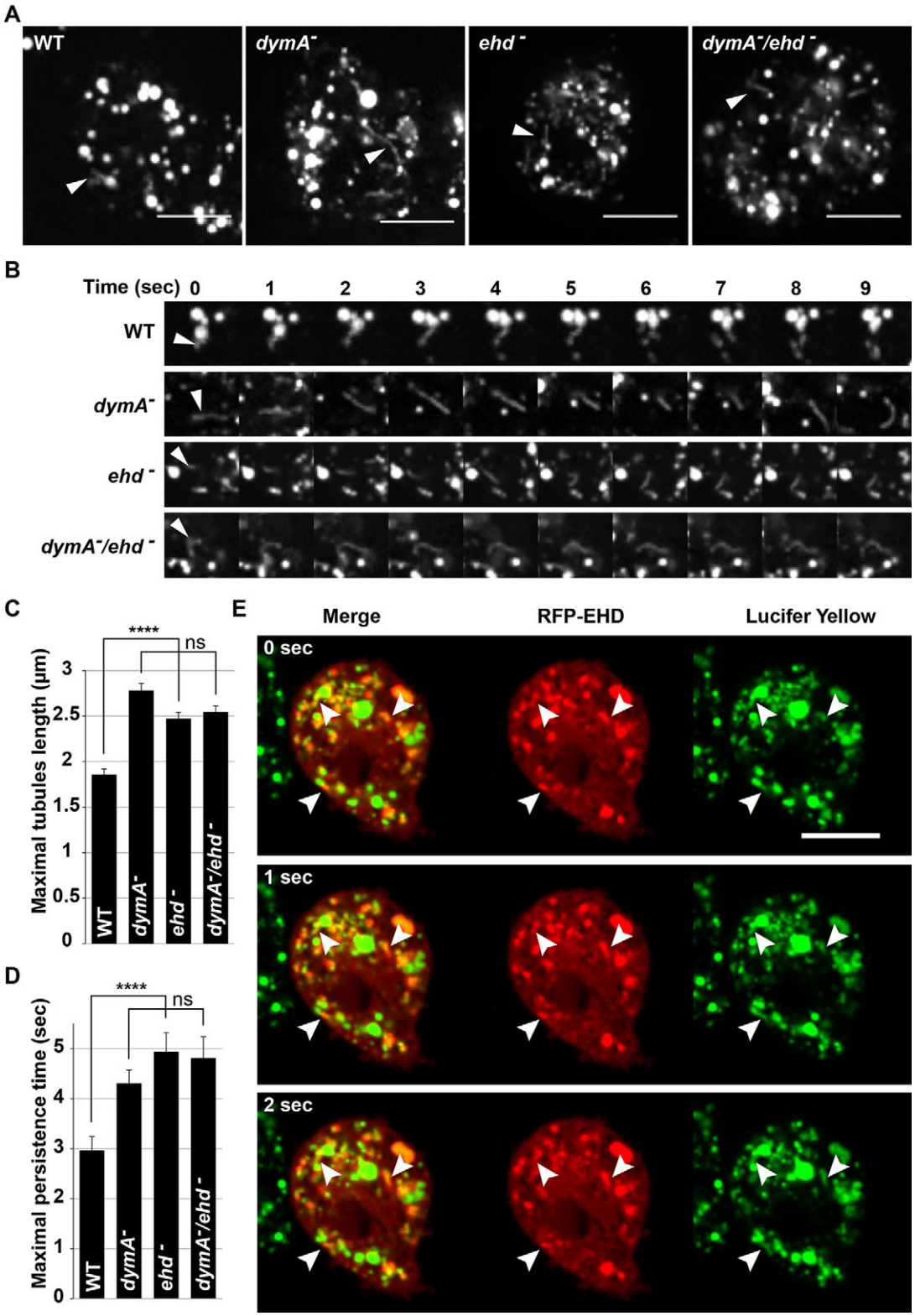

Fig. 7. Endosomal tubules in *ehd*$^{-}$ cells. (A) Morphology of endocytic compartments in WT, *dymA*$^{-}$, *ehd*$^{-}$ and *dymA*$^{-}$*ehd*$^{-}$ cells. Cells were incubated overnight in culture medium containing TRITC–dextran (0.5 mg/ml) to load all endocytic compartments and were observed with spinning disk confocal microscopy. Arrowheads indicate tubular structures. Scale bars: 10 µm. (B) Galleries of images to document the dynamics of tubular structures in the indicated cells. Cells were treated as described in A and imaged every second. Galleries are from Movies 4–7. Quantification of maximal tubule length (C) and maximal time of persistence of tubular structures in the focal plain (D) of at least 100 of these structures was performed using ImageJ. Error bars are s.d. As observed in *dymA*$^{-}$ cells, *ehd*$^{-}$ and *dymA*$^{-}$*ehd*$^{-}$ cells showed longer and more persistent tubular structures than WT cells. (****$P<10^{-4}$; ns, not significant; Student's *t*-test). (E) Endosomal tubules are decorated by RFP–EHD. Cells expressing RFP-tagged EHD were incubated overnight in culture medium containing Lucifer Yellow (0.4 mg/ml) to load all endocytic vacuoles and were then observed with spinning disk confocal microscopy. Three successive images separated by one second are shown and correspond to snapshots of Movie 8. Arrowheads indicate tubular structures. Scale bar: 10 µm.

Journal of Cell Science (2016) 129, 2354-2367 doi:10.1242/jcs.182857

role in phagosome maturation has never been reported. Owing to the unique sorting functions of flotillins, the interplay between flotillins and EHD might be an interesting future research avenue.

EHD and tubule vesiculation

Sorting and transport of cargo from endocytic recycling compartments back to the plasma membrane mainly relies on tubular membranes budding from these endosomes (Maxfield and McGraw, 2004). Mammalian EHDs are reported to either contribute to the formation of these endosomal tubules or to control their scission (Naslavsky and Caplan, 2011). Here, we observed that the length and the time of persistence of endosomal tubules were increased in EHD-depleted cells (Fig. 7). Furthermore, although RFP–EHD localized to the length of short-lived tubules (Fig. 7E), overexpression of RFP–EHD had no major effects on endosomal tubule formation. These results are consistent with a mechanistic role of *D. discoideum* EHD in vesiculation rather than in tubulation of endosomes. What is the molecular basis for this functional specificity? As previously proposed for human EHD1 and EHD3, which show opposite vesiculation and tubulation functions (Cai et al., 2013), EHD-mediated vesiculation in *D. discoideum* might originate from the three-dimensional structure of EHD that is likely to favor vesiculation rather than tubulation. This propensity for vesiculation might be also linked to EHD putative binding partners that provide this feature. No EHD-binding proteins with known membrane tubulation activities were identified in our yeast two-hybrid screen. Although additional experiments would be required to confirm this result, the absence of *D. discoideum* EHD-binding partners with membrane-bending functions might explain its restricted role in vesiculation. Finally, it is unknown whether identical mechanisms are employed for the biogenesis of tubules and vesicles emanating from phagosomes and endosomes. Our results indicate that both DymA and EHD are shared elements for membrane remodeling activities in these different compartments. However, we reveal here that DymA and EHD play specific roles in phagosome maturation, whereas they might have redundant functions in endosomal vesiculation. The molecular basis of these possible differences will have to be further dissected.

MATERIALS AND METHODS

Cell culture, antibodies, immunofluorescence microscopy and endocytosis

D. discoideum strain AX2 was grown at 22°C in HL5c medium. The laboratory strain of *Klebsiella pneumoniae* was also used to grow *D. discoideum*, as reported previously (Alibaud et al., 2008). Antibodies used in this study were mouse monoclonal antibodies against p80 (H161, not commercial; dilution 1:800) (Ravanel et al., 2001), p25 (H72, not commercial; undiluted hybridoma culture supernatant) (Mercanti et al., 2006), vacuolar H^+-ATPase (221-35-2, not commercial; undiluted hybridoma culture supernatant) (Neuhaus et al., 1998) and rabbit polyclonal antibodies against Alix (1:500; Mattei et al., 2005), CatD (1:2000; Journet et al., 1999), DymA (1:2000; Wienke et al., 1999), EHD (anti-p64) (1:5000; Dias et al., 2013), LmpA (1:5000; Karakesisoglou et al., 1999) and MyoB (1:500; Novak et al., 1995). For immunofluorescence analysis, cells were fixed and treated as detailed previously in Dias et al. (2013). The Alexa-Fluor-647-coupled anti-p80 antibody was a kind gift from Pierre Cosson (Centre Médical Universitaire, Geneva, Switzerland). Actin was stained with TRITC-labeled phalloidin (Sigma-Aldrich). Cells were observed with confocal microscopy (Zeiss LSM 510). For nuclei staining, fixed cells were incubated with DAPI for 30 min and observed with a Zeiss AxioImager Z1 photomicroscope. Internalization of fluid phase (Alexa-Fluor-647–dextran; Molecular Probes) or phagocytic particles (YG-fluorescent 1-µm latex beads; Polysciences) was performed as previously described (Lima et al., 2012) and analyzed by performing flow cytometry (FACS Calibur, Becton Dickinson). All flow cytometry data were normalized to protein content.

Plasmids, cell transfections and knockout strains

The EHD coding sequence was cloned into an extrachromosomal inducible expression vector (Veltman et al., 2009). After electroporation, transfectants were selected and maintained in 25 µg/ml hygromycin. Expression was induced by adding 10 µg/ml doxycycline 24 h before analysis. Plasmids encoding VatM–GFP (Clarke et al., 2002) or GFP–DymA (Wienke et al., 1999) were transfected into cells by electroporation, as reported previously (Alibaud et al., 2003). Mutant GFP–DymA-NGS (mutations P573G,F574S) was obtained by PCR mutagenesis, sequenced and cloned into the GFP–DymA expression vector. To obtain the *ehd* (dictyBase ID, DDB_G0282283) knockout vector, the 5′ fragment was amplified from genomic DNA with sense (5′-GGATCCATGAAGAAACTTAATGTTCA-AGAACAA-3′) and antisense (5′ AAGCTTTTATCAATACAATTCTAA-TCTTTTCATCAT-3′) oligonucleotides, and cloned into pBlueScript vector (Stratagene). The 3′ fragment was obtained with PCR using sense (5′-AAGCTTTAATACGATTGGTTCATTCTGGAGTGGACC-3′) and antisense (5′-CTCGAGTTATTGTTGTTGTTGTTGTTGTTGTTGTTG-3′) oligonucleotides, and cloned into pBlueScript containing the 5′ fragment. After sequencing, the knockout vector was completed by inserting the blasticidin or neomycin resistance cassettes between the two 5′ and 3′ fragments. The resulting plasmids were linearized through digestion with restriction enzymes (*Kpn*I and *Not*I) and electroporated into AX2 or *dymA*$^-$ cells. Transformants were selected in the presence of 10 µg/ml blasticidin and/or 10 µg/ml G418. Individual colonies were tested by performing PCR, and the absence of expression of EHD was verified by western blotting with an anti-EHD polyclonal antibody.

Lipid dot blots, GST fusion proteins, pulldowns, anti-GFP immunoprecipitation and liposome-binding assay

Lipid dot blot (Echelon Biosciences, Salt Lake City, UT), GST–EHD fusion protein production in bacteria and GST pulldown assays were performed as described previously (Blanc et al., 2009). Anti-GFP immunoprecipitations were performed using the commercial GFP-Trap system (ChromoTek GmbH, Martinsried, Germany) according to the manufacturer's instructions. Lipids were purchased from Avanti Polar Lipids (Alabaster, AL, USA) – egg L-α-phosphatidylcholine (EPC); 1,2-dioleoyl-sn-glycero-3-phospho-L-serine (DOPS); 1,2-dioleoyl-sn-glycero-3-phospho-(1′-myo-inositol-3′-phosphate) [PI(3)*P*]; 1,2-dioleoyl-sn-glycero-4-phospho-(1′-myo-inositol-4′-phosphate) [PI(4)*P*]; 1,2-dioleoyl-sn-glycero-5-phospho-(1′-myo-inositol-5′-phosphate) [PI(5)*P*]; 1,2-dioleoyl-sn-glycero-3-phospho-(1′-myo-inositol-3′,5′-bisphosphate) [P(3,5)P_2]; and 1,2-dioleoyl-sn-glycero-3-phospho-(1′-myo-inositol-4′,5′-bisphosphate) [PI(4,5)P_2]. Small unilamellar vesicles (SUVs) were prepared as described previously (Daumke et al., 2007). For binding assays, 1 µM GST–EHD and 1.5 mg/ml SUVs were incubated in liposome buffer (20 mM HEPES pH 7.2, 150 mM NaCl, 1 mM $MgCl_2$) for 1 h at room temperature. SUVs were then centrifuged at 20,000 ***g*** for 20 min at room temperature; supernatant and pellet fractions were recovered and analyzed by performing SDS-PAGE electrophoresis.

Glycosidase activity, phagosomal pH and proteolysis activity, and phagosomes purification

Glycosidase activities in cell pellets and extracellular fluid were assessed as previously described (Froquet et al., 2008; Le Coadic et al., 2013). For phagosomal pH measurement, 3-µm carboxylated silica beads coupled to the pH-sensitive fluorophore FITC and to the pH-insensitive fluorophore Alexa-Fluor-594 were used. For phagosomal proteolysis activity analysis, 3-µm carboxylated silica beads coupled to Alexa-Fluor-594 and to BSA labeled with DQ Green at a self-quenching concentration were used. Upon BSA digestion, DQ Green fluorescence increases owing to dequenching. Phagosomal pH and proteolysis activity measurements were performed as described previously (Sattler et al., 2013) using a fluorescence plate reader (Synergy Mx, Biotek, Bad Friedrichshall, Germany). Phagosomes were isolated at different times of maturation, as previously described (Dieckmann et al., 2008). Immunoblots were performed as described previously (Gotthardt et al., 2006), and band intensities were measured using the ImageJ software. For each temporal profile, intensities were normalized by setting the maximal signal obtained to 100%.

Live-cell microscopy

Cells were plated at 30% confluence in a 35-mm iBIDI dish and incubated overnight in HL5c medium. 30 min before imaging, HL5c medium was replaced with low fluorescence medium (LoFlo medium). Then, 3-µm latex beads were washed three times in HL5c and added to the cells at a ratio of two beads per cell. To initiate bead uptake, beads were centrifuged onto the adhered cells for 1 to 2 min at 500 ***g*** at 4°C. Excess medium was removed, and a 1-mm thin 2% agar sheet was placed on top of the cells in order to improve imaging (Sattler et al., 2013). Unless otherwise mentioned, images were then acquired every 30 s to 1 min with a spinning disk confocal system (Intelligent Imaging Innovations, Göttingen, Germany) mounted on an inverted microscope (Leica DMIRE2; Leica, Heerbrugg, Switzerland). To visualize tubules, cells were incubated overnight in 0.5 mg/ml of TRITC-labeled dextran. Cells were then overlaid with a 1-mm thin agar sheet, imaged every second for 3 min as described above. Images were processed using the PureDenoise plugin of the ImageJ software.

Electron microscopy

Cells were fixed for 1 h in 2% glutaraldehyde in HL5c culture medium and then stained for 30 min in 2% osmium with 0.1 M imidazole, as described previously (Barisch et al., 2015). After staining, cells were washed with PBS. Samples were then dehydrated, embedded in Epon resin and processed for conventional electron microscopy. Grids were examined with a Tecnai transmission electron microscope (FEI, Eindhoven, The Netherlands).

Acknowledgements

We thank Dr Jason King (University of Sheffield, UK) for critical reading of the manuscript.

Competing interests

The authors declare no competing or financial interests.

Author contributions

N.G. performed most time-lapse video microscopy, electron microscopy, phagosomal proteolytic activities and pH profile analysis. C.B. conducted liposome co-sedimentation and some phagosomal proteolytic activities and pH profile analysis. N.G. performed liposome co-sedimentation experiments. V.M. wrote the paper. T.S conceived the study, and wrote the paper. F.L. conceived the study, constructed and characterized mutant strains, and wrote the paper.

Funding

This work was funded by the Centre National de la Recherche Scientifique (CNRS); the Université de Montpellier; and also supported by grants from the Fondation ARC pour la Recherche sur le Cancer (to F.L.); the ATIP-AVENIR Program (Institut National de la Santé et de la Recherche Médicale); Conseil Régional Languedoc-Roussillon (to V.M.); and the Swiss National Science Foundation (Schweizerischer Nationalfonds zur Förderung der Wissenschaftlichen Forschung) (to T.S.).

Supplementary information

Supplementary information available online at
http://jcs.biologists.org/lookup/doi/10.1242/jcs.182857.supplemental

References

Akbar, M. A., Tracy, C., Kahr, W. H. A. and Krämer, H. (2011). The full-of-bacteria gene is required for phagosome maturation during immune defense in Drosophila. *J. Cell Biol.* **192**, 383-390.

Alibaud, L., Cosson, P. and Benghezal, M. (2003). Dictyostelium discoideum transformation by oscillating electric field electroporation. *Biotechniques* **35**, 78-80, 82-3.

Alibaud, L., Köhler, T., Coudray, A., Prigent-Combaret, C., Bergeret, E., Perrin, J., Benghezal, M., Reimmann, C., Gauthier, Y., van Delden, C. et al. (2008). Pseudomonas aeruginosa virulence genes identified in a Dictyostelium host model. *Cell Microbiol.* **10**, 729-740.

Aubry, L., Klein, G., Martiel, J. L. and Satre, M. (1993). Kinetics of endosomal pH evolution in Dictyostelium discoideum amoebae. Study by fluorescence spectroscopy. *J. Cell Sci.* **105**, 861-866.

Bahl, K., Naslavsky, N. and Caplan, S. (2015). Role of the EHD2 unstructured loop in dimerization, protein binding and subcellular localization. *PLoS ONE* **10**, e0123710.

Barisch, C., Paschke, P., Hagedorn, M., Maniak, M. and Soldati, T. (2015). Lipid droplet dynamics at early stages of Mycobacterium marinum infection in Dictyostelium. *Cell. Microbiol.* **17**, 1332-1349.

Blanc, C., Charette, S. J., Mattei, S., Aubry, L., Smith, E. W., Cosson, P. and Letourneur, F. (2009). Dictyostelium Tom1 participates to an ancestral ESCRT-0 complex. *Traffic* **10**, 161-171.

Cai, B., Giridharan, S. S. P., Zhang, J., Saxena, S., Bahl, K., Schmidt, J. A., Sorgen, P. L., Guo, W., Naslavsky, N. and Caplan, S. (2013). Differential roles of C-terminal Eps15 homology domain proteins as vesiculators and tubulators of recycling endosomes. *J. Biol. Chem.* **288**, 30172-30180.

Caplan, S., Naslavsky, N., Hartnell, L. M., Lodge, R., Polishchuk, R. S., Donaldson, J. G. and Bonifacino, J. S. (2002). A tubular EHD1-containing compartment involved in the recycling of major histocompatibility complex class I molecules to the plasma membrane. *EMBO J.* **21**, 2557-2567.

Carnell, M., Zech, T., Calaminus, S. D., Ura, S., Hagedorn, M., Johnston, S. A., May, R. C., Soldati, T., Machesky, L. M. and Insall, R. H. (2011). Actin polymerization driven by WASH causes V-ATPase retrieval and vesicle neutralization before exocytosis. *J. Cell Biol.* **193**, 831-839.

Charette, S. J. and Cosson, P. (2006). Exocytosis of late endosomes does not directly contribute membrane to the formation of phagocytic cups or pseudopods in Dictyostelium. *FEBS Lett.* **580**, 4923-4928.

Chen, D., Jian, Y., Liu, X., Zhang, Y., Liang, J., Qi, X., Du, H., Zou, W., Chen, L., Chai, Y. et al. (2013). Clathrin and AP2 are required for phagocytic receptor-mediated apoptotic cell clearance in Caenorhabditis elegans. *PLoS Genet.* **9**, e1003517.

Chen, D., Xiao, H., Zhang, K., Wang, B., Gao, Z., Jian, Y., Qi, X., Sun, J., Miao, L. and Yang, C. (2010). Retromer is required for apoptotic cell clearance by phagocytic receptor recycling. *Science* **327**, 1261-1264.

Clarke, M., Kohler, J., Arana, Q., Liu, T., Heuser, J. and Gerisch, G. (2002). Dynamics of the vacuolar H(+)-ATPase in the contractile vacuole complex and the endosomal pathway of Dictyostelium cells. *J. Cell Sci.* **115**, 2893-2905.

Clarke, M., Maddera, L., Engel, U. and Gerisch, G. (2010). Retrieval of the vacuolar H+-ATPase from phagosomes revealed by live cell imaging. *PLoS ONE* **5**, e8585.

Confalonieri, S. and Di Fiore, P. P. (2002). The Eps15 homology (EH) domain. *FEBS Lett.* **513**, 24-29.

Daumke, O., Lundmark, R., Vallis, Y., Martens, S., Butler, P. J. and McMahon, H. T. (2007). Architectural and mechanistic insights into an EHD ATPase involved in membrane remodelling. *Nature* **449**, 923-927.

de Beer, T., Carter, R. E., Lobel-Rice, K. E., Sorkin, A. and Overduin, M. (1998). Structure and Asn-Pro-Phe binding pocket of the Eps15 homology domain. *Science* **281**, 1357-1360.

Derivery, E., Sousa, C., Gautier, J. J., Lombard, B., Loew, D. and Gautreau, A. (2009). The Arp2/3 activator WASH controls the fission of endosomes through a large multiprotein complex. *Dev. Cell* **17**, 712-723.

Dias, M., Blanc, C., Thazar-Poulot, N., Ben Larbi, S., Cosson, P. and Letourneur, F. (2013). Dictyostelium ACAP-A is an ArfGAP involved in cytokinesis, cell migration and actin cytoskeleton dynamics. *J. Cell Sci.* **126**, 756-766.

Dieckmann, R., Gopaldass, N., Escalera, C. and Soldati, T. (2008). Monitoring time-dependent maturation changes in purified phagosomes from Dictyostelium discoideum. *Methods Mol. Biol.* **445**, 327-337.

Dieckmann, R., von Heyden, Y., Kistler, C., Gopaldass, N., Hausherr, S., Crawley, S. W., Schwarz, E. C., Diensthuber, R. P., Cote, G. P., Tsiavaliaris, G. et al. (2010). A myosin IK-Abp1-PakB circuit acts as a switch to regulate phagocytosis efficiency. *Mol. Biol. Cell* **21**, 1505-1518.

Fairn, G. D. and Grinstein, S. (2012). How nascent phagosomes mature to become phagolysosomes. *Trends Immunol.* **33**, 397-405.

Froquet, R., Cherix, N., Birke, R., Benghezal, M., Cameroni, E., Letourneur, F., Mosch, H.-U., De Virgilio, C. and Cosson, P. (2008). Control of cellular physiology by TM9 proteins in yeast and Dictyostelium. *J. Biol. Chem.* **283**, 6764-6772.

Gopaldass, N., Patel, D., Kratzke, R., Dieckmann, R., Hausherr, S., Hagedorn, M., Monroy, R., Krüger, J., Neuhaus, E. M., Hoffmann, E. et al. (2012). Dynamin A, Myosin IB and Abp1 couple phagosome maturation to F-actin binding. *Traffic* **13**, 120-130.

Gotthardt, D., Warnatz, H. J., Henschel, O., Brückert, F., Schleicher, M. and Soldati, T. (2002). High-resolution dissection of phagosome maturation reveals distinct membrane trafficking phases. *Mol. Biol. Cell* **13**, 3508-3520.

Gotthardt, D., Blancheteau, V., Bosserhoff, A., Ruppert, T., Delorenzi, M. and Soldati, T. (2006). Proteomics fingerprinting of phagosome maturation and evidence for the role of a Galpha during uptake. *Mol. Cell. Proteomics* **5**, 2228-2243.

Grant, B. D. and Caplan, S. (2008). Mechanisms of EHD/RME-1 protein function in endocytic transport. *Traffic* **9**, 2043-2052.

Grant, B., Zhang, Y., Paupard, M.-C., Lin, S. X., Hall, D. H. and Hirsh, D. (2001). Evidence that RME-1, a conserved C. elegans EH-domain protein, functions in endocytic recycling. *Nat. Cell Biol.* **3**, 573-579.

Guetta, D., Langou, K., Grunwald, D., Klein, G. and Aubry, L. (2010). FYVE-dependent endosomal targeting of an arrestin-related protein in amoeba. *PLoS ONE* **5**, e15249.

Jakobsson, J., Ackermann, F., Andersson, F., Larhammar, D., Low, P. and Brodin, L. (2011). Regulation of synaptic vesicle budding and dynamin function by an EHD ATPase. *J. Neurosci.* **31**, 13972-13980.

Jenne, N., Rauchenberger, R., Hacker, U., Kast, T. and Maniak, M. (1998). Targeted gene disruption reveals a role for vacuolin B in the late endocytic pathway and exocytosis. *J. Cell Sci.* **111**, 61-70.

Journet, A., Chapel, A., Jehan, S., Adessi, C., Freeze, H., Klein, G. and Garin, J. (1999). Characterization of Dictyostelium discoideum cathepsin D. *J. Cell Sci.* **112**, 3833-3843.

Jovic, M., Naslavsky, N., Rapaport, D., Horowitz, M. and Caplan, S. (2007). EHD1 regulates beta1 integrin endosomal transport: effects on focal adhesions, cell spreading and migration. *J. Cell Sci.* **120**, 802-814.
Karakesisoglou, I., Janssen, K.-P., Eichinger, L., Noegel, A. A. and Schleicher, M. (1999). Identification of a suppressor of the Dictyostelium profilin-minus phenotype as a CD36/LIMP-II homologue. *J. Cell Biol.* **145**, 167-181.
Kinchen, J. M., Doukoumetzidis, K., Almendinger, J., Stergiou, L., Tosello-Trampont, A., Sifri, C. D., Hengartner, M. O. and Ravichandran, K. S. (2008). A pathway for phagosome maturation during engulfment of apoptotic cells. *Nat. Cell Biol.* **10**, 556-566.
Klockow, B., Tichelaar, W., Madden, D. R., Niemann, H. H., Akiba, T., Hirose, K. and Manstein, D. J. (2002). The dynamin A ring complex: molecular organization and nucleotide-dependent conformational changes. *EMBO J.* **21**, 240-250.
Le Coadic, M., Froquet, R., Lima, W. C., Dias, M., Marchetti, A. and Cosson, P. (2013). Phg1/TM9 proteins control intracellular killing of bacteria by determining cellular levels of the Kil1 sulfotransferase in Dictyostelium. *PLoS ONE* **8**, e53259.
Lee, S., Uchida, Y., Wang, J., Matsudaira, T., Nakagawa, T., Kishimoto, T., Mukai, K., Inaba, T., Kobayashi, T., Molday, R. S. et al. (2015). Transport through recycling endosomes requires EHD1 recruitment by a phosphatidylserine translocase. *EMBO J.* **34**, 669-688.
Lima, W. C., Leuba, F., Soldati, T. and Cosson, P. (2012). Mucolipin controls lysosome exocytosis in Dictyostelium. *J. Cell Sci.* **125**, 2315-2322.
Lin, S. X., Grant, B., Hirsh, D. and Maxfield, F. R. (2001). Rme-1 regulates the distribution and function of the endocytic recycling compartment in mammalian cells. *Nat. Cell Biol.* **3**, 567-572.
Maniak, M. (2003). Fusion and fission events in the endocytic pathway of Dictyostelium. *Traffic* **4**, 1-5.
Marchetti, A., Lelong, E. and Cosson, P. (2009). A measure of endosomal pH by flow cytometry in Dictyostelium. *BMC Res. Notes* **2**, 7.
Mattei, S., Ryves, W. J., Blot, B., Sadoul, R., Harwood, A. J., Satre, M., Klein, G. and Aubry, L. (2005). Dd-Alix, a conserved endosome-associated protein, controls Dictyostelium development. *Dev. Biol.* **279**, 99-113.
Maxfield, F. R. and McGraw, T. E. (2004). Endocytic recycling. *Nat. Rev. Mol. Cell Biol.* **5**, 121-132.
Meister, M. and Tikkanen, R. (2014). Endocytic trafficking of membrane-bound cargo: a flotillin point of view. *Membranes* **4**, 356-371.
Mercanti, V., Charette, S. J., Bennett, N., Ryckewaert, J.-J., Letourneur, F. and Cosson, P. (2006). Selective membrane exclusion in phagocytic and macropinocytic cups. *J. Cell Sci.* **119**, 4079-4087.
Mintz, L., Galperin, E., Pasmanik-Chor, M., Tulzinsky, S., Bromberg, Y., Kozak, C. A., Joyner, A., Fein, A. and Horowitz, M. (1999). EHD1—an EH-domain-containing protein with a specific expression pattern. *Genomics* **59**, 66-76.
Naslavsky, N. and Caplan, S. (2011). EHD proteins: key conductors of endocytic transport. *Trends Cell Biol.* **21**, 122-131.
Naslavsky, N., Rahajeng, J., Chenavas, S., Sorgen, P. L. and Caplan, S. (2007). EHD1 and Eps15 interact with phosphatidylinositols via their Eps15 homology domains. *J. Biol. Chem.* **282**, 16612-16622.
Naslavsky, N., McKenzie, J., Altan-Bonnet, N., Sheff, D. and Caplan, S. (2009). EHD3 regulates early-endosome-to-Golgi transport and preserves Golgi morphology. *J. Cell Sci.* **122**, 389-400.
Neuhaus, E. M., Horstmann, H., Almers, W., Maniak, M. and Soldati, T. (1998). Ethane-freezing/methanol-fixation of cell monolayers: a procedure for improved preservation of structure and antigenicity for light and electron microscopies. *J. Struct. Biol.* **121**, 326-342.
Neuhaus, E. M., Almers, W. and Soldati, T. (2002). Morphology and dynamics of the endocytic pathway in Dictyostelium discoideum. *Mol. Biol. Cell* **13**, 1390-1407.
Novak, K. D., Peterson, M. D., Reedy, M. C. and Titus, M. A. (1995). Dictyostelium myosin I double mutants exhibit conditional defects in pinocytosis. *J. Cell Biol.* **131**, 1205-1221.
Olswang-Kutz, Y., Gertel, Y., Benjamin, S., Sela, O., Pekar, O., Arama, E., Steller, H., Horowitz, M. and Segal, D. (2009). Drosophila Past1 is involved in endocytosis and is required for germline development and survival of the adult fly. *J. Cell Sci.* **122**, 471-480.
Pant, S., Sharma, M., Patel, K., Caplan, S., Carr, C. M. and Grant, B. D. (2009). AMPH-1/Amphiphysin/Bin1 functions with RME-1/Ehd1 in endocytic recycling. *Nat. Cell Biol.* **11**, 1399-1410.
Park, L., Thomason, P. A., Zech, T., King, J. S., Veltman, D. M., Carnell, M., Ura, S., Machesky, L. M. and Insall, R. H. (2013). Cyclical action of the WASH complex: FAM21 and capping protein drive WASH recycling, not initial recruitment. *Dev. Cell* **24**, 169-181.
Prelich, G. (2012). Gene overexpression: uses, mechanisms, and interpretation. *Genetics* **190**, 841-854.
Rahajeng, J., Giridharan, S. S., Naslavsky, N. and Caplan, S. (2010). Collapsin response mediator protein-2 (Crmp2) regulates trafficking by linking endocytic regulatory proteins to dynein motors. *J. Biol. Chem.* **285**, 31918-31922.
Ravanel, K., de Chassey, B., Cornillon, S., Benghezal, M., Zulianello, L., Gebbie, L., Letourneur, F. and Cosson, P. (2001). Membrane sorting in the endocytic and phagocytic pathway of Dictyostelium discoideum. *Eur. J. Cell Biol.* **80**, 754-764.
Sattler, N., Monroy, R. and Soldati, T. (2013). Quantitative analysis of phagocytosis and phagosome maturation. *Methods Mol. Biol.* **983**, 383-402.
Solis, G. P., Hulsbusch, N., Radon, Y., Katanaev, V. L., Plattner, H. and Stuermer, C. A. O. (2013). Reggies/flotillins interact with Rab11a and SNX4 at the tubulovesicular recycling compartment and function in transferrin receptor and E-cadherin trafficking. *Mol. Biol. Cell* **24**, 2689-2702.
Takei, K., Haucke, V., Slepnev, V., Farsad, K., Salazar, M., Chen, H. and De Camilli, P. (1998). Generation of coated intermediates of clathrin-mediated endocytosis on protein-free liposomes. *Cell* **94**, 131-141.
Veltman, D. M., Keizer-Gunnink, I. and Haastert, P. J. V. (2009). An extrachromosomal, inducible expression system for Dictyostelium discoideum. *Plasmid* **61**, 119-125.
Wienke, D. C., Knetsch, M. L. W., Neuhaus, E. M., Reedy, M. C. and Manstein, D. J. (1999). Disruption of a dynamin homologue affects endocytosis, organelle morphology, and cytokinesis in Dictyostelium discoideum. *Mol. Biol. Cell* **10**, 225-243.
Yeung, T., Heit, B., Dubuisson, J.-F., Fairn, G. D., Chiu, B., Inman, R., Kapus, A., Swanson, M. and Grinstein, S. (2009). Contribution of phosphatidylserine to membrane surface charge and protein targeting during phagosome maturation. *J. Cell Biol.* **185**, 917-928.
Zhang, J., Naslavsky, N. and Caplan, S. (2012a). EHDs meet the retromer: complex regulation of retrograde transport. *Cell. Logist.* **2**, 161-165.
Zhang, J., Naslavsky, N. and Caplan, S. (2012b). Rabs and EHDs: alternate modes for traffic control. *Biosci. Rep.* **32**, 17-23.
Zhang, J., Reiling, C., Reinecke, J. B., Prislan, I., Marky, L. A., Sorgen, P. L., Naslavsky, N. and Caplan, S. (2012c). Rabankyrin-5 interacts with EHD1 and Vps26 to regulate endocytic trafficking and retromer function. *Traffic* **13**, 745-757.
Zhu, G.-d., Salazar, G., Zlatic, S. A., Fiza, B., Doucette, M. M., Heilman, C. J., Levey, A. I., Faundez, V. and L'Hernault, S. W. (2009). SPE-39 family proteins interact with the HOPS complex and function in lysosomal delivery. *Mol. Biol. Cell* **20**, 1223-1240.

Supplementary material

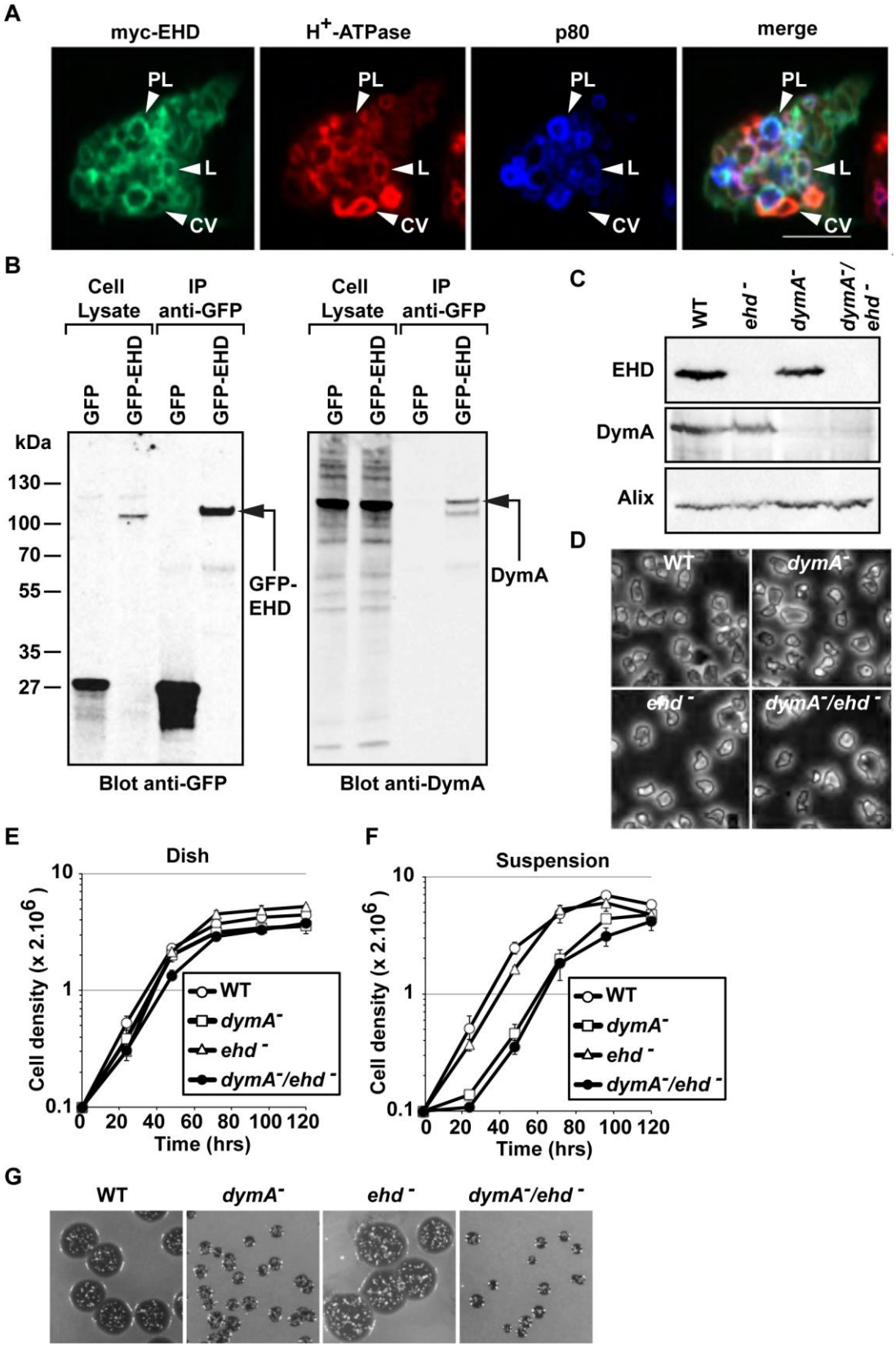

Fig. S1. Intracellular localization of myc-tagged-EHD, interaction between DymA and GFP-EHD, and characterization of mutant strains.
(A) Cells expressing myc-tagged-EHD (green) were processed for immunofluorescence and analyzed by confocal microscopy. Lysosomes (L) are identified as H^+-ATPase-positive (red) and p80-positive (blue) vacuoles. Post-lysosomes (PL) are detected as H^+-ATPase-negative and p80-positive endosomal structures. The contractile vacuole (CV) is positive for the H^+-ATPase and presents a characteristic morphology. Bar, 5 μm. **(B)** Co-immunoprecipitation between DymA and GFP-EHD. Lysates of cells expressing GFP alone or GFP-EHD where incubated with beads coupled to an anti-GFP antibody. Bound proteins were revealed by immunoblotting with anti-DymA and anti-GFP antibodies as indicated. **(C)** Loss of expression of EHD in *ehd*$^-$ and double *dymA*$^-$/*ehd*$^-$ cells was verified by western blot. Whole cell lysates of the indicated cell lines (106 cells/lane) were analyzed by western blot with rabbit polyclonal antibodies to EHD and DymA. Identical amounts of protein were loaded in each lane as verified by immunoblotting with an anti-Alix antibody. **(D)** Cells were observed by phase-contrast microscopy to reveal size differences between cell lines. Growth curves of cells cultivated in Petri-dish **(E)** or in suspension **(F)** for 5 days in culture medium. **(G)** The indicated cell lines were grown on lawns of *Klebsiella pneumonia* for 5 days.

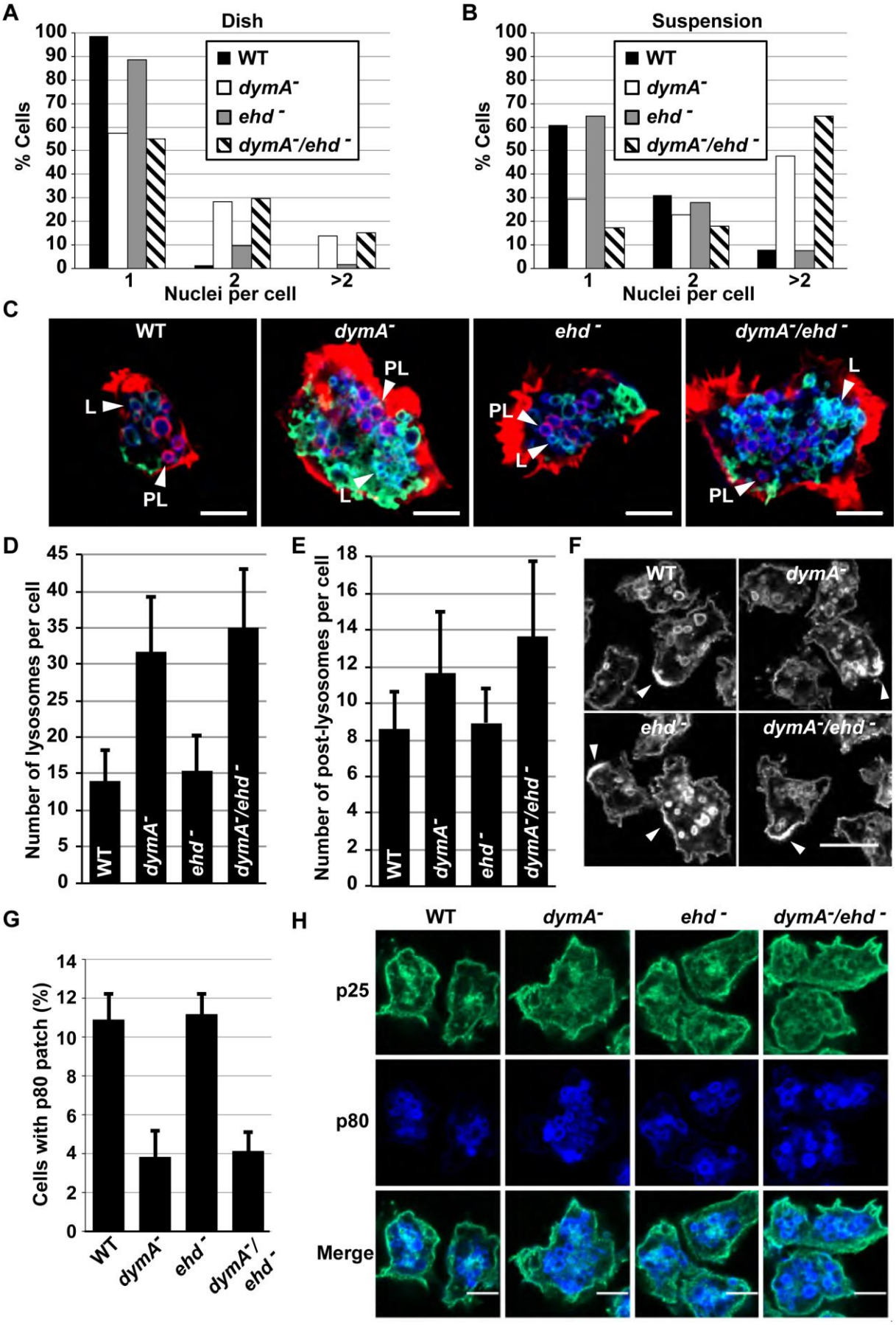

Fig. S2. Analysis of cytokinesis, endocytic compartments and exocytic functions in *dymA*$^-$, *ehd*$^-$, and *dymA*$^-$/*ehd*$^-$ cells.
(A) Histograms showing the distribution of nuclei/cell among the indicated cells grown in Petri-dish and in suspension **(B)** for 4 days at 180 r.p.m. Results shown are from one representative experiment out of three (n=500 cells). **(C)** Endocytic compartments analyzed by immunofluorescence. The indicated cells were processed for immunofluorescence and analyzed by confocal microscopy. Actin is shown in red, H^+-ATPase in green, and p80 protein in blue. Lysosomes (L) are identified as H^+-ATPase-positive, p80-positive and actinnegative vacuoles. Post-lysosomes (PL) are detected as H^+-ATPase-negative, p80-positive and actin-negative endosomal structures. **(D, E)** Numbers of lysosomes (D) and postlysosomes (E) in mutant cells were determined by confocal microscope analysis of z-stacks of cells (n=20) stained as in (C). Features of lysosomes and post-lysosomes in *ehd*$^-$ and *dymA*$^-$/*ehd*$^-$ were comparable to that of parental WT and *dymA*$^-$ strains respectively **(F)** The efficacy 2 of post-lysosomes fusion with the plasma membrane was carefully evaluated by quantifying cell surface p80 patches (arrowheads) transiently formed by the fusion of p80-enriched postlysosomes with the cell surface Cells were treated for immunofluorescence and stained with an anti-p80 antibody before confocal microscopy analysis. Bar, 10μm. **(G)** Quantification of the number of cells with p80 patches (expressed at the percentage of total cells). At least two hundred cells were observed from three independent experiments. This assay did not reveal any defects resulting from the absence of EHD in WT cells or aggravation of *dymA*$^-$ phenotypes in *dymA*$^-$/*ehd*$^-$ cells. **(H)** Endocytic recycling compartments analyzed by immunofluorescence. Since human EHD1 has been reported to control recycling from early endosomes to the plasma membrane, we tested the localization of p25, a marker of recycling endososomes in *D. discoideum* (Charette et al., 2006). The indicated cells were labeled with anti-p25 (recycling endosomes, green) and anti-p80 (lysosomes and post-lysosomes, blue) antibodies, and analyzed by confocal microscopy. No apparent localization defects were visualized by immunofluorescence analysis, although we cannot formally exclude a role of EHD in this recycling pathway not detected here. Bars, 5 μm.

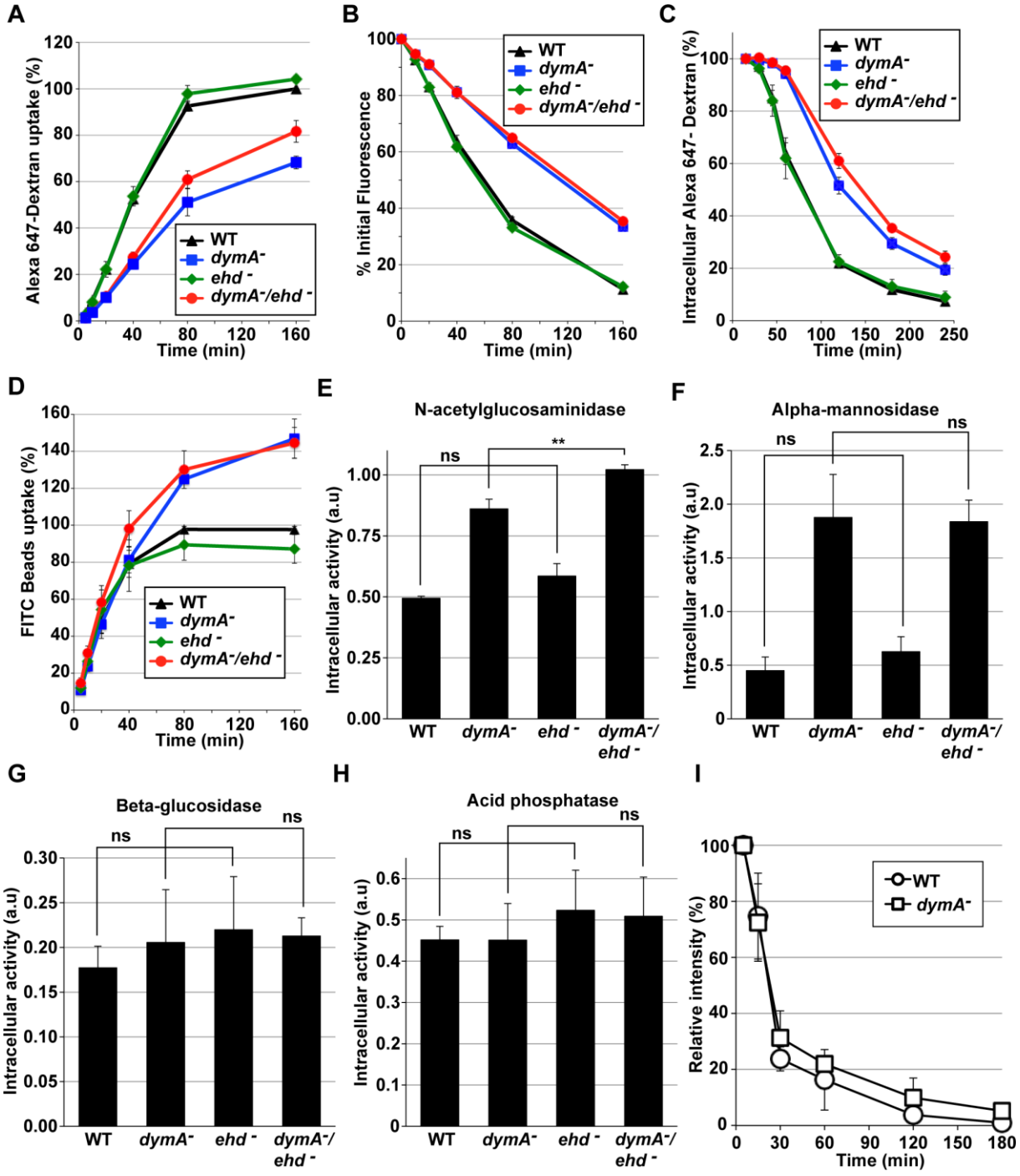

Fig. S3. Analysis of endocytic functions and lysosomal enzymes activities in *dymA*$^-$, *ehd*$^-$, and *dymA*$^-$ /*ehd*$^-$ cells.

(A) To analyze fluid-phase uptake, cells were incubated with Dextran coupled to Alexa-647 for the indicated periods of time, washed and then analyzed by flow cytometry. Results are expressed as the percent of the maximum fluorescence in WT cells. **(B)** For exocytosis analysis, cells were incubated overnight in Petri dishes with Alexa-647-dextran to load all endocytic compartments, washed, and incubated with dextran-free medium. At the indicated time points, the fluorescence remaining in cells was measured by flow cytometry and expressed as the percent of the initial fluorescence. **(C)** The intracellular transit time of fluidphase was determined by incubation of cells with Alexa-647-dextran for a 10 min pulse,

and intracellular fluorescence was recorded after different chase periods. The percent of maximal fluorescence for each cell type was calculated. **(D)** To determine phagocytic rates, cells were incubated with 1 μm YG-labeled beads and internal fluorescence was analyzed by flow cytometry for the indicated periods of time. Data are expressed as the percent of maximal uptake in WT cells. All flow cytometry data are normalized to protein content and represent the average and s.e.m. of three independent experiments. Uptake, transit time within endocytic compartments, exocytosis of Dextran, and phagocytosis rates were similar in mutant and parental cells. **(E-H)** Intracellular activities of lysosomal N-acetylglucosaminidase 3 (E), alpha-mannosidase (F), beta-glucosidase (G), and acid phosphatase (H) were assessed in cellular pellets of the indicated cell lines grown in HL5c culture medium. WT and *ehd*$^-$ cells showed similar enzymatic activities. Remarkably, enzymatic activities were increased in *dymA*$^-$ cells compared to WT and *ehd*$^-$ cells, but not further increased in *dymA*$^-$/*ehd*$^-$ double mutant except for N-acetylglucosaminidase activity that was slightly increased in *dymA*$^-$/*ehd*$^-$ cells compared to *dymA*$^-$ cells. All data are normalized to protein content and represent the average and s.e.m. of three independent experiments. (**, P<0.005; ns, not significant). **(I)** Quantification from two western blot profiles of EHD content in phagosomes containing latex beads isolated at different times of maturation in WT and *dymA*$^-$ cells. Results are expressed as percentage of the maximal signals obtained (open circles, WT cells; open squares, *dymA*$^-$ cells). Identical profiles are observed in WT and *dymA*$^-$ cells.

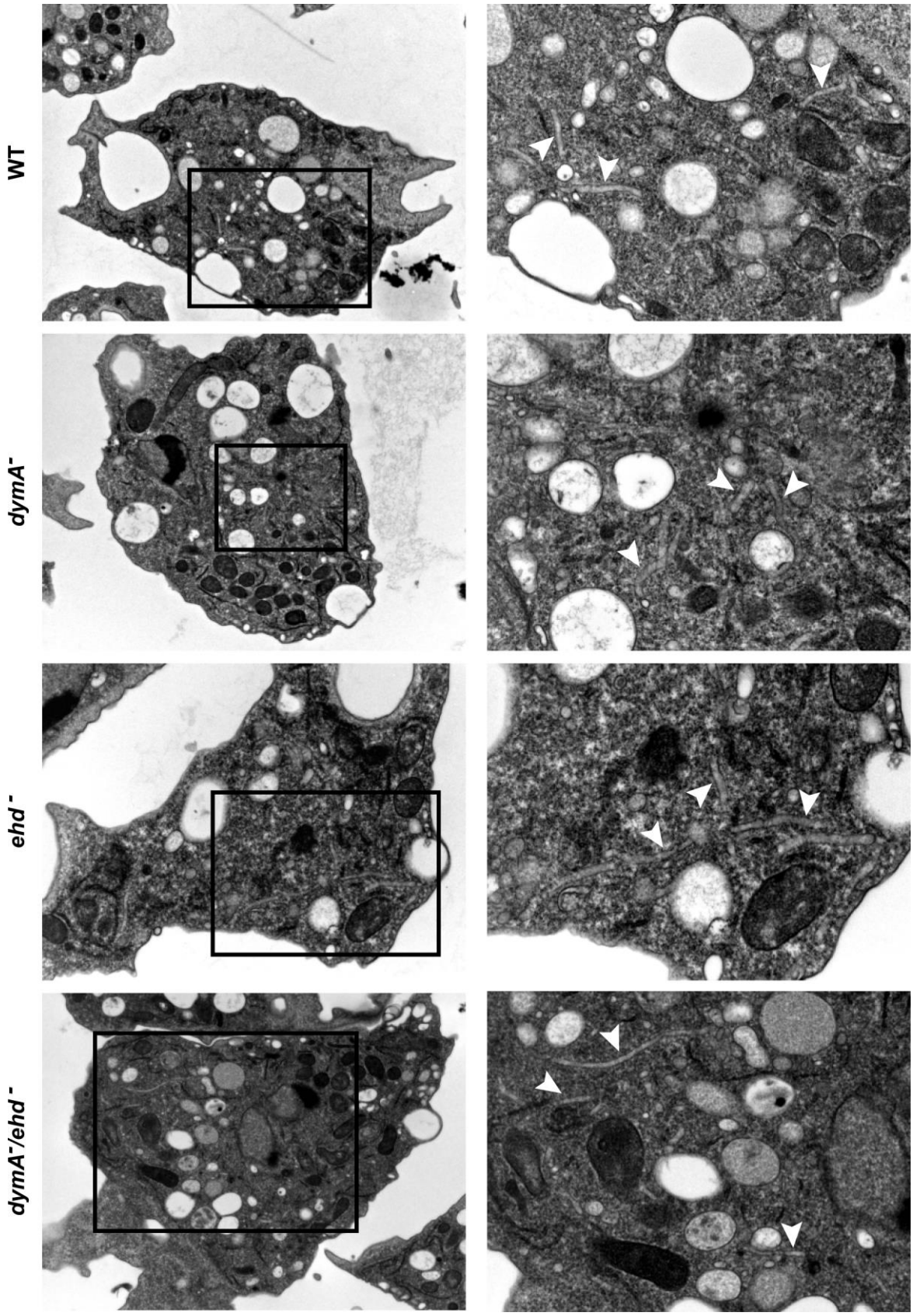
WT
dymA-
ehd-
dymA-/ehd-

Fig. S4. Electron microscopy analysis of mutant cells.
The indicated cells were examined by transmission electron microscopy. Ultrastructural analysis of endosomal tubules did not reveal any marked morphological differences of tubules observed in WT and mutant cells. Right panels correspond to higher magnification of selected area (black frames) in images shown in left panels. White arrowheads indicate tubular structures.

Supplementary movie 1. Temporal recruitment of RFP-EHD and GFP-DymA to phagosomes containing latex beads in WT cells.

Supplementary movie 2. Temporal recruitment of H^+-ATPase (VatM-GFP) to phagosomes containing latex beads in WT cells.

Supplementary movie 3. Temporal recruitment of H^+-ATPase (VatM-GFP) to phagosomes containing latex beads in *ehd*$^-$ cells.

Supplementary movie 4. Dynamics of tubular structures of WT cells incubated with TRITCdextran and imaged every second by spinning disc confocal microscopy.

Supplementary movie 5. Dynamics of tubular structures of *dymA*$^{-}$ cells incubated with TRITC-dextran and imaged every second by spinning disc confocal microscopy.

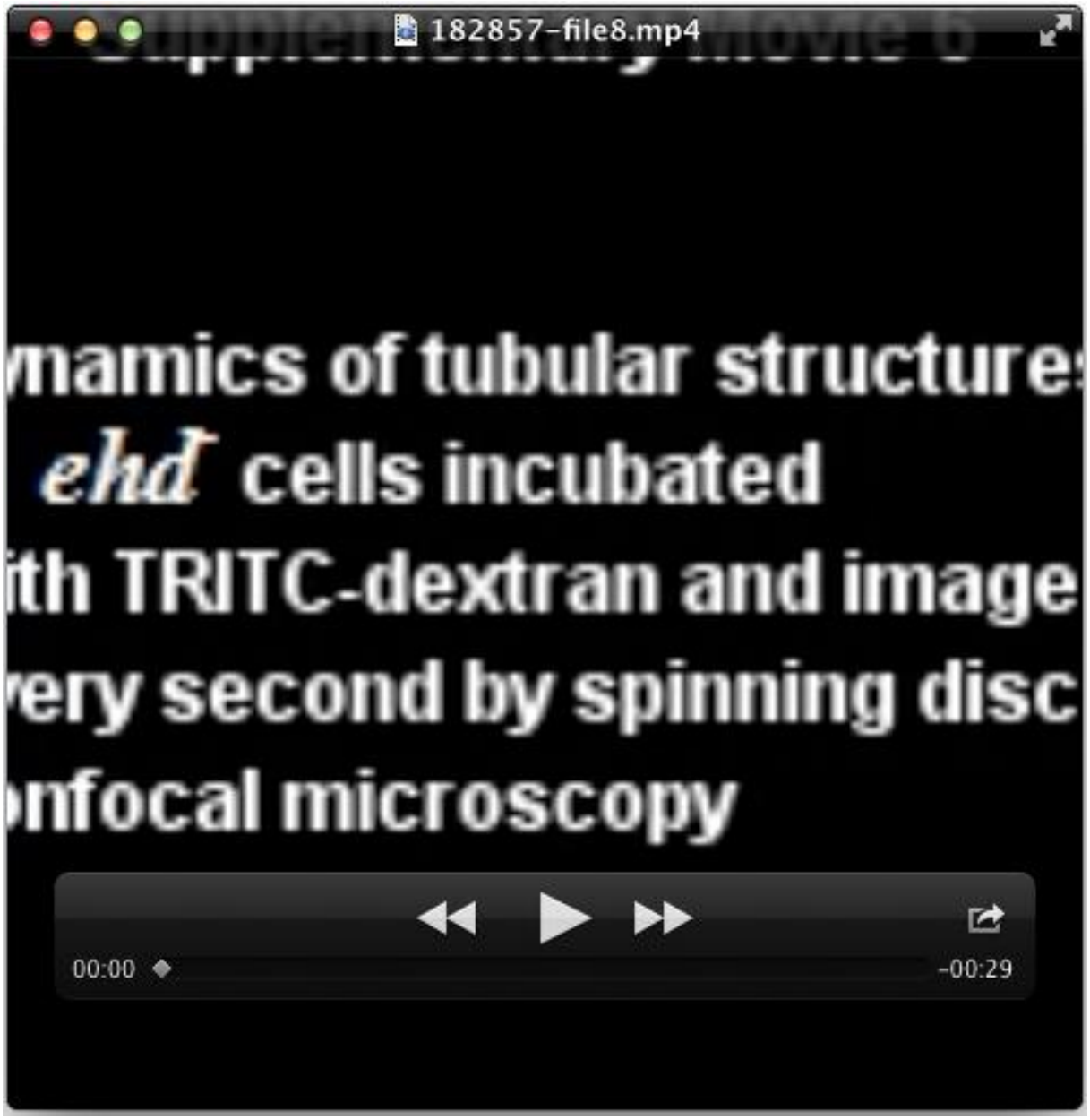

Supplementary movie 6. Dynamics of tubular structures of *ehd*$^{-}$ cells incubated with TRITCdextran and imaged every second by spinning disc confocal microscopy.

Supplementary movie 7. Dynamics of tubular structures of *dymA*$^{-}$*/ehd*$^{-}$ cells incubated with TRITC-dextran and imaged every second by spinning disc confocal microscopy.

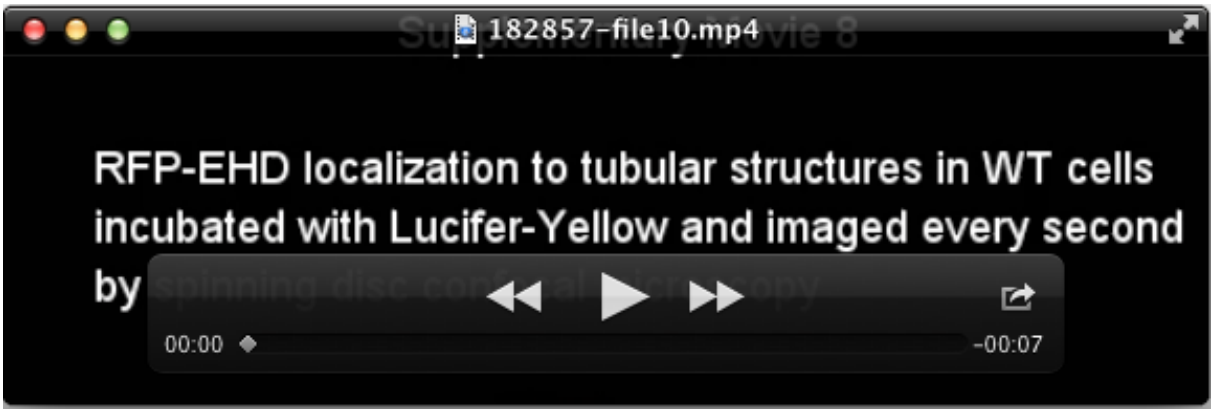

Supplementary movie 8. RFP-EHD localization to tubular structures in WT cells incubated with Lucifer-Yellow and images every second by spinning disc confocal microscopy.

Table S1: Results of the yeast two-hybrid screen made with the EH domain of EHD as a bait.

A yeast two-hybrid screen with the EH domain of *D. discoideum* EHD as a bait was performed to test 65.8 millions interactions (Hybrigenics SA, France). The interaction confidence (lane 1, rated from A to D) was computed based on the comparison between the number of independent prey fragments found for an interaction (lane 2) and the chance of finding them at random (provided by Hybrigenics SA). Gene names, NCBI accession numbers and comments are indicated (lane 3).

Confidence	Number of preys	Gene name, accession number and comments
A	10	abpF; XM_630062.1; hypothetical actin binding protein (abpF)
A	43	dymA; XM_637020.1; dynamin like protein (dymA)
A	49	glycoside hydrolase family 18 protein; XM_639146.1; putative di-N-acetylchitobiase
A	7	hypothetical protein; XM_636670.1; histone deacetylase family protein
A	18	hypothetical protein; XM_628885.1; NDT80/PhoG-like protein
A	49	hypothetical protein; XM_629573.1; similar to human VPS33B-interacting protein
A	30	hypothetical protein; XM_001134571.1; CCR4-NOT transcription complex subunit 11
B	6	CDK family protein kinase protein kinase; XM_637304.1
B	32	hypothetical protein; XM_634021.1; Stearoyl-CoA 9-Desaturase
B	11	hypothetical protein; XM_639165.1
C	4	cpsf1; XM_635423.1; hypothetical protein, CPSF domain-containing protein
C	3	hypothetical protein; XM_632248.1
D	1	ap1g1; XM_635290.1; clathrin-adaptor gamma chain (ap1g1)
D	2	Arf GTPase activating protein; XM_642017.1
D	22	cprD; XM_636871.1; cysteine protease 4 (cprD)
D	1	dhcA; XM_638093.1; cytoplasmic dynein heavy chain (dhcA)
D	2	drnA-2; XM_639305.1; putative RNase III (drnA-2)
D	2	drpp20; XM_631285.1; RNase P protein subunit (drpp20)
D	1	epnA; XM_630177.1; epsin
D	1	etfb; XM_636966.1; electron transfer flavoprotein beta subunit
D	4	gefE; XM_641388.1; Ras guanine nucleotide exchange factor (gefE)
D	1	hypothetical protein; XM_628892.1
D	2	hypothetical protein; XM_629895.1
D	3	hypothetical protein; XM_632292.1
D	1	hypothetical protein; XM_633422.1
D	2	hypothetical protein; XM_637859.1
D	2	hypothetical protein; XM_639675.1; Similar to Homo sapiens mucin 2
D	2	hypothetical protein; XM_641487.1
D	1	hypothetical protein; XM_642581.1; DNA topoisomerase 2-associated protein PAT1
D	1	krsB; XM_642369.1; calpain-like cysteine protease (krsB)
D	1	lysS; XM_635585.1; lysine-tRNA ligase (lysS) mRNA
D	3	nacB; XM_635431.1; NAC domain-containing protein
D	1	naglu; XM_629755.1; alpha-N-acetylglucosaminidase (naglu)
D	1	PA14 domain-containing protein; XM_631395.1
D	1	protein phosphatase 2C-like domain-containingprotein; XM_633707.2
D	7	putative protein serine/threonine kinase; XM_629346.1
D	1	putative transmembrane protein; XM_633076.1
D	3	Ras GTPase domain-containing protein; XM_629168.1
D	6	vps13E; XM_641945.1; vacuolar protein sorting-associated protein 13 family protein